---

**Article:**
Pontin, M. orcid.org/0000-0002-4363-0649 and Damian, D.D. orcid.org/0000-0002-0595-0182 (2024) Multimodal soft valve enables physical responsiveness for preemptive resilience of soft robots. Science Robotics, 9 (92). ISSN 2470-9476

https://doi.org/10.1126/scirobotics.adk9978

---

**Title:** Multimodal Soft Valve Enables Physical Responsiveness for Pre-emptive Resilience of Soft Robots

**Authors:**

Marco Pontin,[1,2]* Dana D. Damian,[1,2,3]*

**Affiliations:**

[1]Department of Automatic Control and Systems Engineering, University of Sheffield; Sheffield, UK.

[2]Sheffield Robotics, University of Sheffield, Sheffield, UK.

[3]Insigneo Institute for in silico Medicine, University of Sheffield, Sheffield, UK.

*Corresponding author. Email: mpontin1@sheffield.ac.uk, d.damian@sheffield.ac.uk.

**Abstract:** Resilience is crucial for the self-preservation of biological systems: humans recover from wounds thanks to an immune system that autonomously enacts a multi-staged response to promote healing. Similar passive mechanisms can enable pneumatic soft robots to overcome common faults such as bursts originating from punctures or overpressurization. Recent technological advancements, ranging from fault-tolerant controllers for robot reconfigurability to self-healing materials, paved the way for robot resilience. However, these techniques respectively require powerful processors and large data sets, or external hardware. How to extend the operational lifespan of damaged soft robots with minimal computational and physical resources remains unclear.

In this study, we demonstrate a multimodal pneumatic soft valve capable of passive resilient reactions, triggered by the faults, to prevent or isolate damage in soft robots. In its forward operation mode, the valve, requiring a single supply pressure, isolates punctured soft inflatable elements from the rest of the soft robot as fast as 21 milliseconds. In its reverse operation mode, the valve can passively protect robots against overpressurization caused by external disturbances, avoiding plastic deformations and bursts. Furthermore, the two modes combined enable the creation of an endogenously controlled valve capable of autonomous burst isolation. We demonstrate the passive and quick response, and the possibility of monolithic integration of the soft valve in grippers and crawling robots. The approach proposed in this study provides a distributed small-footprint alternative to controller-based resilience and is expected to help soft robots achieve uninterrupted long-lasting operation, facilitating their widespread adoption.

**One-Sentence Summary:** Multimodal soft valves provide pneumatic soft robots with passive, embodied, and autonomous fault isolation and prevention.

## INTRODUCTION

Soft robots demonstrate advanced capabilities such as high deformation, inherent shock absorbance, and light structures, compared to those of classical rigid robots, because of the compliance of their bodies. As such, they are promising for applications in human–robot interaction, medical robots, and marine and space robots (*1–7*). Most soft robots are fluidically actuated because such systems entail reduced complexity in fabrication and integration. In particular, pneumatic actuators, which consist of one or more chambers, are connected to a pressure input to enable pressurization, and, consequently, robotic motion. In addition, electromechanical components such as valves and control logic and pressure sensors are required for pressure regulation.

Despite their promising potential, fluidic soft robots are prone to failure just as much as traditional robots. Bursts from cuts or overpressurization represent a common and critical mode of failure, which leads to unresponsive robots and reduces their reliability and potential for adoption (*8*, *9*). Vulnerabilities in technologies are a well-known challenge, with recognized unfavorable economic consequences and risks to humans. The classical fault-tolerant framework (*10*) built around rigid machines relies on complex control algorithms to achieve behavior adaptation after a critical fault, to salvage as much capability of the system as possible (*11*, *12*). In the same framework, reconfigurable and self-assembling systems have been researched to grant spare parts to robots in cases of breakages (*13–15*). However, these approaches assume discrete, addressable points of failure such as sensors, actuators, or links, making it difficult to scale these techniques to high-degree-of-freedom machines or the entire body of a robot. In addition, the entire framework is based on a centralized architecture in which the controller makes decisions based on feedback from various sensors, often requiring precise models or extensive training, which is usually computationally demanding.

Soft robots introduce an embodied approach to fault recovery, i.e., self-healing materials, which exploit chemically enabled repairs (such as reversible Diels–Alder bonds and H-bonds). This approach is highly distributed and does not require a model or extensive computations (*8*, *16–21*). Although self-healing materials are fundamental to soft robotic resilience, they suffer from some limitations. For example, the healing can be time consuming, and external stimuli or human intervention are sometimes required to complete the healing process. Further, fluidic actuators must remain deflated to their neutral state for the healing to occur and, if part of the material is removed during the fault, the chances of recovery are diminished drastically.

Resilience in living creatures shows a level of nuance that robots continue to lack. For instance, humans benefit from a multi-stage process to treat injuries, activated by the innate immune system. A wounded finger triggers a tightly coordinated cascade of reactions at different timescales (*22–24*). First, a local inflammatory response is generated to prevent blood loss and protect against infection. In the medium-term, growth factors are released, triggering cell proliferation and skin regeneration. While these reactions take place passively and unconsciously, humans adopt cautious behaviors meant to aid in the recovery of the injured finger. Therefore, biological organisms provide inspiration for developing responsive resilience strategies for autonomous fault isolation, so that damage does not propagate further and the system is maintained operational until full recovery is achieved through methods such as material-level healing. Soft-matter-embodied mechanisms that can react to a fault instantly and passively, to stop further harm to the robot or its environment, are therefore needed; however, this remains an unexplored area. Valves, which constitute fundamental computational elements in fluidic systems, could be used for such purposes.

Soft valves have evolved considerably, fueled by research into realizing soft-matter digital and analogue fluidic components to control soft robots. Microfluidic research has demonstrated the possibility of replicating complex digital logic circuits (*25–27*) while achieving compact designs (*28*). In addition, recent advancements in 3D-printing techniques and materials have permitted the merging of control logic and actuators into one unit, leading to the creation of monolithic soft robots (*29–31*), thus decreasing their production costs and time. Recent work showing soft-matter valves, pumps, and controllers has demonstrated the possibility of creating entirely soft robots (*32–35*). In particular, the development of valves, guided by the parallels between

fluidic and electric system modeling (*36*), targets the replication of functionalities obtained with CMOS technologies for logic and computational purposes (*37, 38*). Other soft-matter valve designs have exploited mechanical phenomena such as bistability (*39*, *40*) and buckling (*41*) to create oscillators for robot control and locomotion (*42*). Furthermore, the combination of state-of-the-art inkjet printing and monopropellant fluids (*43*) has led to the development of soft robots that include fluidic controllers and onboard pressure generation (*29*). Despite these advancements in replicating complex behaviors through ingenious fluidic circuits, using such circuits for soft robot resilience assumes that the robot is equipped with pressure sensors and valves for every functional fluidic chamber, has centralized control, and a quick response time. All of these factors increase the hardware and computational burdens.

The use of soft valves to endow robots with matter-embedded responsive resilience is a recent, understudied development. In (*44*), our group designed and characterized a valve that can automatically detect bursts and perform isolation, whereas, in (*45*), a soft-fuse valve for realizing the same purpose was proposed. In this paper, inspired by the passive and autonomous nature of mechanisms observed in living beings, we present a fully soft valve that exhibits multimodal behavior to achieve passive distributed resilience in pneumatic soft robots. The passive autonomous burst detection and isolation behavior is triggered in the forward operation mode (FOM) of the soft valve, whereas in the reverse operation mode (ROM), the soft valve passively detects and protects against the overpressurization of the actuators. In both cases, the valve exploits pressure differences induced by the faults to trigger its own response, either preventing the failure, or avoiding its propagation to the system. Finally, the multimodality of the valve is used to create an endogenously controlled two-stage soft valve that can generate its own control signal, avoiding the need for an externally actuated line, while maintaining burst detection and isolation capabilities. The resilient capabilities enabled by the multimodal soft valve are exhibited in several manipulation and locomotion demonstrations. The innovations in this study demonstrate embodied fluidic circuits that pre-emptively respond to damages in soft robots, thus extending their operational lifespan, with minimal resources, and facilitating the development of an embodied unified platform for bioinspired treatment of malfunctions.

## RESULTS

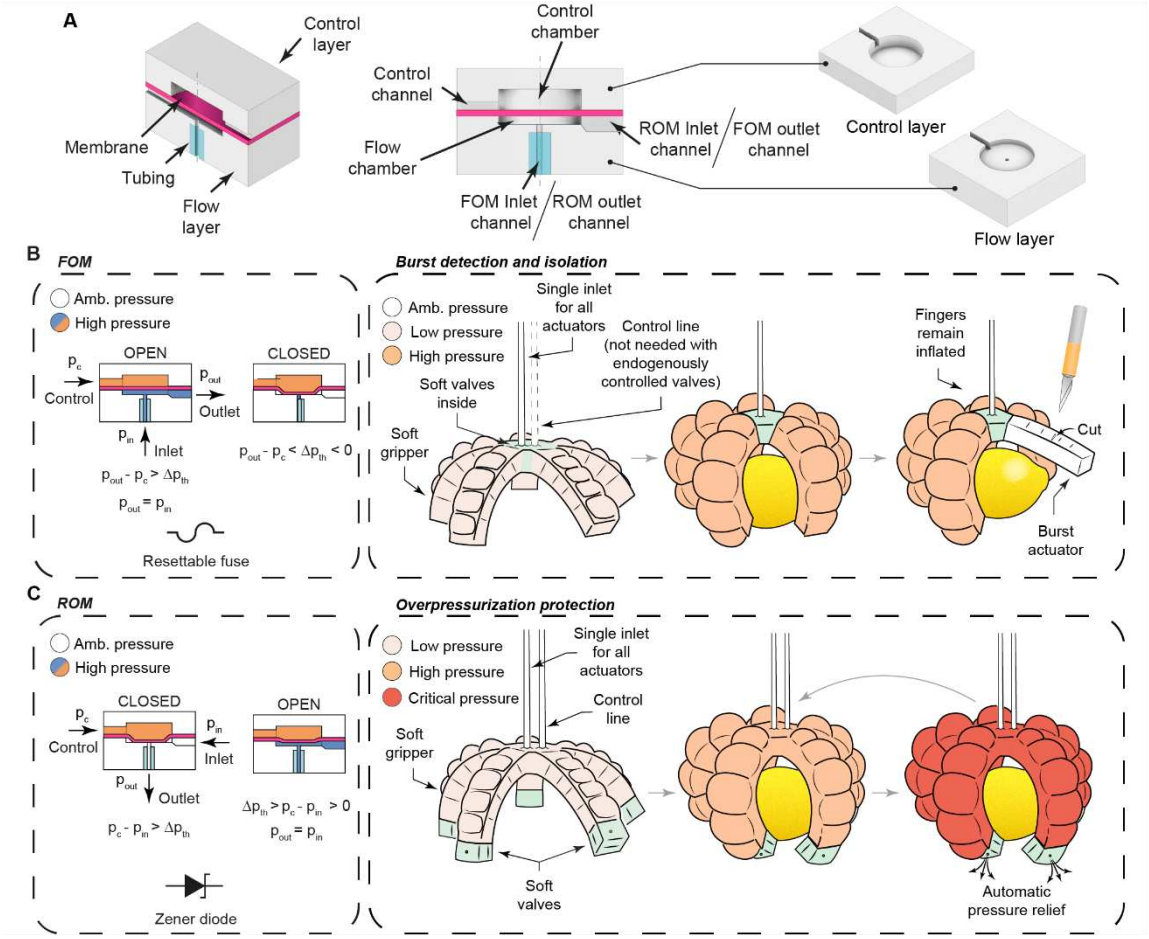


**Fig. 1. Details of the soft valve and possible applications. (A)** Internal structure of the valve and main components. **(B)** The soft valve, configured in forward operation mode (FOM) can act as a resettable fuse. When paired with soft actuators, the valve can automatically detect and isolate bursts, preventing a single actuator fault from affecting the whole system. **(C)** The reverse operation mode (ROM), the second mode of operation of the valve, turns the valve into the equivalent of a Zener diode. In this configuration, the valve can protect actuators against damage from overpressurization, caused either by controller error or by external disturbances.

The pneumatic soft valve shown in Fig. 1A consists of three functional layers. The membrane separates the control layer, where the control chamber resides, from the flow layer, which connects the main inlet and outlet ports. The integrated tubing in the valve acts as a constraint, preventing the associated section of the channel from expanding when pressurized and serves as a localized resistance for the airflow. The single-material design and compact structure enable simple integration into existing soft robots. The geometry and position of the internal channels were selected to grant multimodality, i.e. different operation modes depending on how the valve is connected to a soft actuator, with a single supply pressure. In particular, we distinguish between a forward operation mode (FOM) and a reverse operation Mode (ROM).

In FOM, the narrow vertical channel serves as the inlet (Fig. 1B). When a sufficiently high pressure difference is reached between the control pressure $p_c$ and outlet pressure $p_{out}$ ($p_c > p_{out}$), the membrane deforms and obstructs the inlet channel, thereby separating the inlet from the outlet (closed condition). In this mode, the valve can be considered as the fluidic equivalent of a resettable fuse. If the valve's outlet is paired with a Soft Inflatable Element (SIE), such as a pneumatic actuator or sensor, passive autonomous burst detection and isolation can be achieved. The burst causes the pressure level underneath the membrane to drop suddenly, leading the membrane to deform downward and obstruct the inlet channel, isolating the faulty SIE from the rest of the system. Instrumental in achieving this result is the high-impedance of the inlet channel, which decouples the inlet and outlet pressures (fig. S1).

In ROM, the narrow channel serves as the outlet, as shown Fig. 1C. The valve starts out closed and later opens when the pressure difference between the chambers on either side of the membrane, $p_c - p_{in}$, drops below a threshold value $\Delta p_{th}$ dependent on the geometry and material properties of the valve. Under these conditions, the deformed membrane no longer obstructs the outlet channel and air can discharge through the valve. In this mode, the valve acts as the equivalent of a Zener diode and, as such, if the valve's inlet is connected to an SIE, it can be used to protect it against overpressurization events.

Multimodality is achieved thanks to the asymmetric geometry of the valve. The control pressure acts on the same surface of the membrane, independent of the operating mode. In contrast, the inlet pressure acts on different areas, depending on the mode. In FOM, when the valve is closed, the area is equal to that of the inlet channel tubing, so the valve can remain closed, even when the inlet and control pressures are equal. In ROM, the pressure acts on the side area of the deformed membrane that is not in contact with the bottom of the flow layer chamber. This change in the active area causes the valve to open, even when $p_{in}$ is lower than $p_c$. This multimodality enables the creation of an endogenously controlled (EC) soft valve capable of self-tuning operation. By combining two soft valves in a two-stage stacked assembly, this version of the soft valve can generate its own control signal, adapting to the inflation transient of the SIE it is paired to. Consequently, passive burst detection and isolation functionality is achieved without an external control line being present.

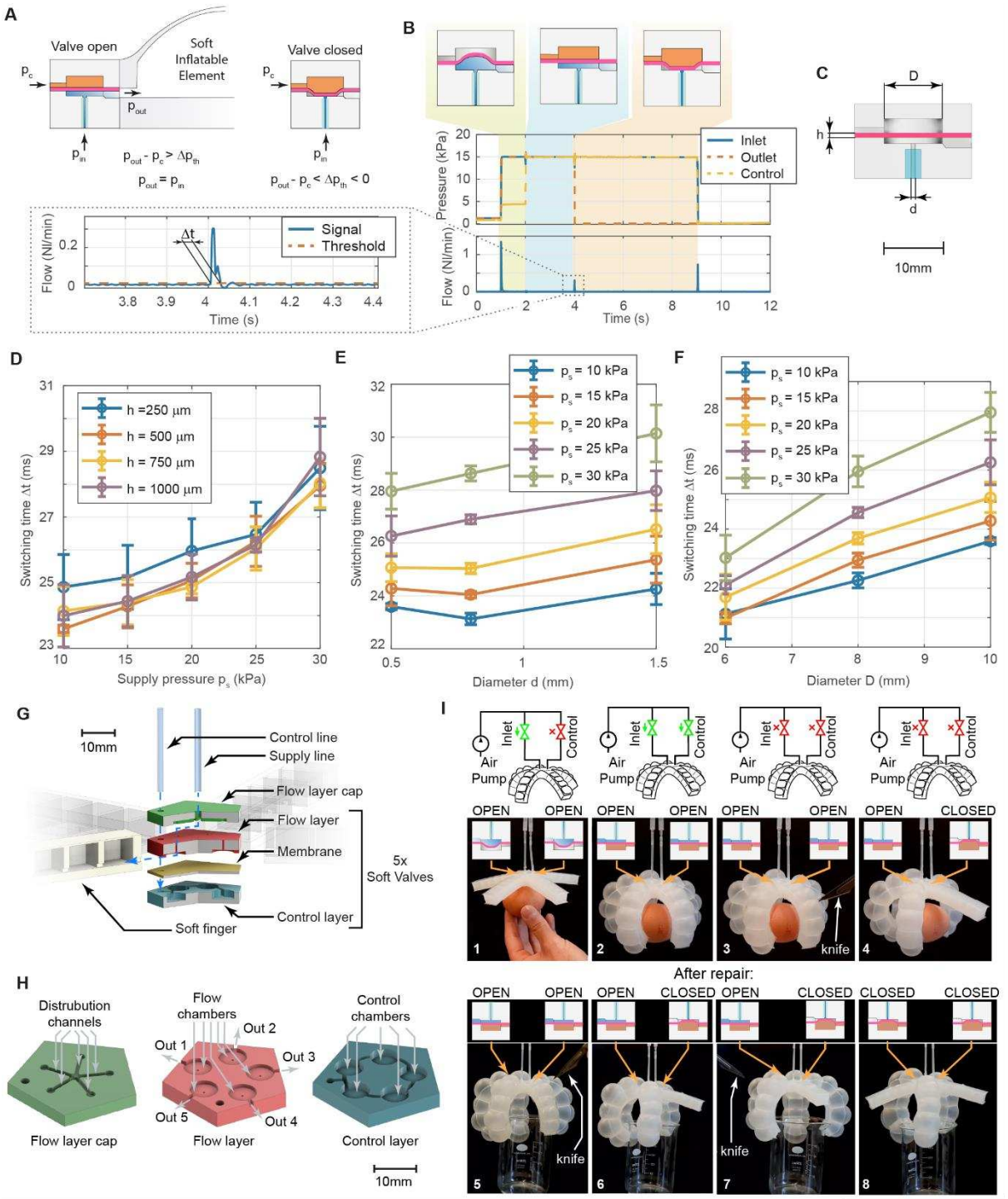


**Fig. 2. FOM behavior characterization and demonstration.** (**A**) Working principle of the FOM behavior. (**B**) Example experiment used to evaluate the valve's reaction time upon a simulated burst (for $D$ = 10 mm, $d$ = 0.5 mm, $h$ = 500 µm). The beginning and end of the flow rate spike are used to compute the switching time $\Delta t$. (**C**) Internal structure of the valve and relevant geometrical parameters. (**D**) Switching time of soft valves with different membrane thicknesses ($D$ = 10 mm, $d$ = 0.5 mm). Error bars in plots indicate the average standard deviation obtained in the trials. (**E**) Narrower inlet channels provide higher input impedance, leading to faster switching times ($D$ = 10 mm, $h$ = 500 µm). (**F**) Smaller $D$ and lower supply pressures translates into faster, more reactive valves ($d$ = 0.5 mm and $h$ =500 µm). **(G)** Internal

structure of the five-finger soft gripper with integrated soft valves ($D$ = 6 mm, $d$ = 0.5 mm, $h$ = 500 μm). Only one supply and one control channel are needed to control the gripper and achieve the burst isolation capability, therefore limiting hardware requirements and control logic complexity. **(H)** Structure of the palm integrating the soft valves. **(I)** Demonstration of the burst detection and isolation capabilities. First, the gripper is inflated and isolated from the supply (steps 1 and 2). One of the fingers is then burst with a precision knife (step 3), but the gripper maintains its grasp on the egg it is holding, thanks to the action of the soft valve connected to the finger (step 4). The faulty finger is repaired using a thin layer of glue and then the gripper is reinflated to grasp a glass beaker (steps 5 and 6). Two fingers are then burst while maintaining the object suspended, showing that more than one finger can fail and the fault detection and isolation still works, independently for each finger (steps 7 and 8).

***Forward operation mode characterization***

In FOM, the valve is positioned between the main pressure source and the SIE and it requires two external signals, inlet and control, at the same supply pressure level $p_s$, for operation (Fig. 2A). A representative burst detection and isolation experiment used to characterize the valve's response time (see the Materials and Methods section for details) is presented in Fig. 2B. The flow layer was pressurized first, followed by the control layer. Because the same pressure $p_s$ acted on both sides of the membrane, the valve remained open for further inflation of the SIE. When a burst occurred (t = 4.0 s), the pressure underneath the membrane dropped quickly, due to the asymmetric distribution of the internal fluidic resistances, causing the membrane to deform, obstruct the inlet, and isolate the outlet. The pressure difference between the two sides of the membrane depends on the ratio of the inlet to the outlet resistance within the soft valve (fig. S2). After the burst, the equilibrium equation for the membrane can be written as $\frac{\pi}{4}\left[p_c\left(D^2 - {d_c}^2\right) - d^2(p_c - p_{in})\right] - fm = 0$, where $D$, $d$, $d_c$, and $fm$ represent the membrane diameter (Fig. 2C and fig. S3), inlet channel diameter, diameter of the contact area between the membrane and the bottom of the flow layer chamber, and elastic force associated with the deformed membrane, respectively. After the burst, the valve remained closed until the control signal was removed.

The valve requires a quick response time and sufficient input impedance to operate correctly for burst isolation. To understand the effects of the internal geometry of the valve, we investigated the effect of the membrane thickness $h$ and both diameters $d$ and $D$ on the switching time $\Delta t$. For the range that was tested, the membrane thickness did not alter the performance in a significant manner (average p-value of one-way ANOVA was p = 0.22, table S1), with all valves averaging a switching time of 25.11 ms (SD = 1.99 ms) (Fig. 2D). More pronounced changes were observed when comparing the different internal geometries. As expected, narrower inlet channels led to faster switching times due to higher input impedance. The largest channel ($d$ = 1.5 mm) averaged 27.1 ms across the supply pressure levels, compared to 25.8 ms for the thinnest one (Fig. 2E). However, the largest change in performance was observed by decreasing the diameter $D$ of the chamber (smaller, more reactive membrane) (Fig. 2F), with an average difference of 3.64 ms between the fastest ($D$ = 6 mm) and slowest ($D$ = 10 mm) geometries and an overall 17.6% improvement (at 30 kPa). Furthermore, the valve's operation under deformation was tested (Supplementary Methods and fig. S4): the valve operated reliably for up to 17% unidirectional compressive strain with a 1000 μm membrane or up to 25% strain with a 250 μm membrane. Lastly, the valve resumed its normal behavior as soon as the external load was removed. In terms of long-term

reliability, lifetime experiments on three soft valves showed no noticeable change in performance after 5000 cycles (Supplementary methods and fig. S5).

***Burst detection and isolation in a five-finger pneumatic soft gripper***

A five-finger elastomeric gripper was used to demonstrate the functionality of the valve in FOM. As shown in Fig. 2G, each finger consists of a Pneu-Net-type actuator (*46*) that bends upon inflation. The fingers are connected to a palm that incorporates one soft valve for each finger (Fig. 2H). All valves are configured in FOM and only two inlets to the system, one for the inflation of the gripper and the other for the pressurization of the control channel, are required, shared among all five valves.

The gripper was inflated to grasp an uncooked egg. Meanwhile, the control channel was pressurized, activating the burst detection and isolation functionality (Fig. 2I, steps 1 and 2, and movie S1). When one finger contacted a sharp object, it burst suddenly, causing the corresponding soft valve to switch and isolate it from the other fingers. As a result, the remaining four fingers maintained their grasp on the object, preventing it from falling (steps 3 and 4). The hole in the faulty finger was sealed using a thin layer of Sil-Poxy glue, and the gripper was reused to grasp a different object (step 5). This time, two fingers were punctured, yet the gripper maintained a firm grasp on the object (steps 6 through 8), further proving the independence between the fingers.

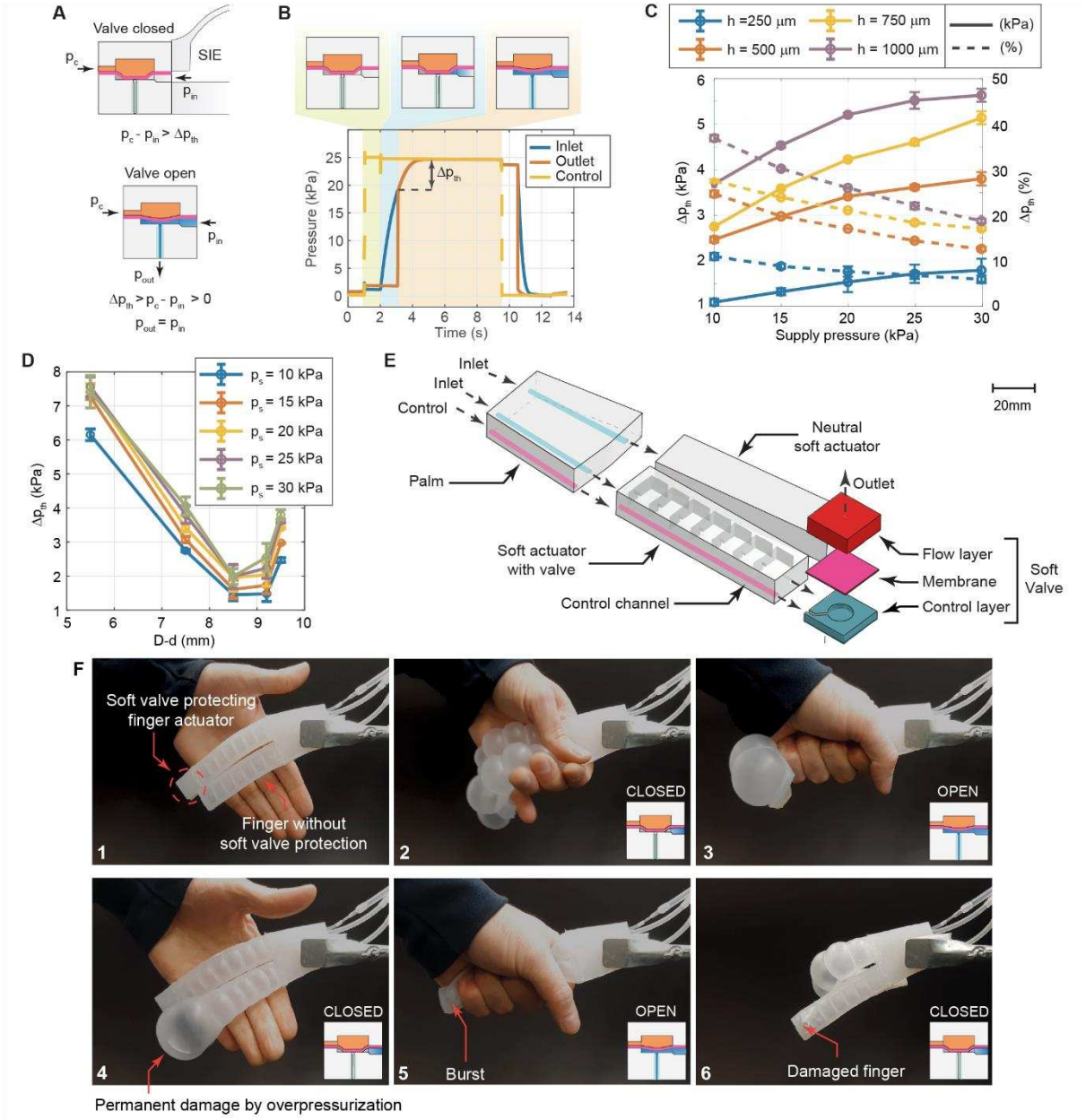


**Fig. 3. ROM behavior characterization and demonstration. (A)** Working principle of the valve's ROM behavior. **(B)** Representative experiment demonstrating the working principle of the valve and its characterization (for $D$ = 6 mm, $d$ = 0.5 mm, $h$ = 500 µm). **(C)** Effect of different membrane thicknesses with $D$ = 10 mm and $d$ = 0.5 mm on $\Delta p_{th}$. Error bars in plots indicate the average standard deviation obtained in the trials. **(D)** The parameter $D$ - $d$ is used as the metric to compare various geometries of the valve. The best performing one, minimum of the curves, was obtained with a difference $D$ - $d$ = 8.5 mm. **(E)** Structure of the two-finger soft hand with all the relevant components and connections. **(F)** Demonstration showing the overpressurization protection capabilities of the ROM configured soft valve. Only the top finger is being protected by the soft valve. Upon inflation, the fingers are squeezed, causing irreparable damage to the unprotected finger (steps 1 through 4). The same finger then bursts after a second run of the experiment (step 5), while the finger protected by the valve still performs the same as upon the first inflation (step 6).

***Reverse operation mode characterization***

In ROM, the control channel starts out pressurized at pressure $p_s$ and the deformed membrane obstructs the narrow outlet channel (valve closed). The second external input is represented by the inlet channel supplied with the same $p_s$. Once pc-pin reaches a threshold value $\Delta p_{th}$, the membrane can no longer obstruct the outlet and the soft valve opens (Fig. 3A). Contrary to what occurs in FOM, in ROM, the equilibrium equation for the deformed membrane is $\frac{\pi}{4}(p_c - p_{in})\left(D^2 - {d_c}^2\right) - fm = 0$ (fig. S3). The ROM behavior of the soft valve is experimentally captured in Fig. 3B. The control channel was pressurized and immediately reached the supply pressure value $p_s$. The inlet channel was then activated. As the inlet pressure increased, the outlet pressure remained at ambient pressure, indicating that the outlet was isolated from the inlet. When the condition $p_c - p_{in} < \Delta p_{th}$ was reached, the valve opened and the outlet pressure $p_{out}$ suddenly rose, matching the value of $p_{in}$. The stability of the valve near the threshold pressure difference was verified by checking for unintended autonomous switching of the soft valve (fig. S6).

Analysis of the effect of the membrane thickness and control pressure showed that, for the same control pressure, thicker membranes required lower values of $p_{in}$ (larger $\Delta p_{th}$) for the valve to open (Fig. 3C). These results can be explained by the superposition of two effects. Thicker membranes deform less at the same control pressure, leaving more side area exposed to the effect of the inlet pressure $p_{in}$. The second effect is that of *fm*, which increases with membrane thickness and pressure $p_c$, lowering the threshold pressure required for the valve to open. A slight upward trend is present in the results, irrespective of the membrane thickness; however, the change in $\Delta p_{th}$ is always less than 2.5 kPa. The downward slope observed in the percentage results, obtained as $\frac{\Delta p_{th}}{p_s}$, demonstrates that this increase was more than compensated for by the increase in the corresponding supply pressure. In addition, thinner membranes showed a more uniform, flattened performance across the various supply pressures: an overall change of 0.7 kPa in $\Delta p_{th}$ was observed for the 250 μm membrane, while this increased to 2.4 kPa with a 750 μm thick membrane.

The comparison of different internal geometries indicated that both diameters *D* and *d* affect the valve's performance (fig. S7); however, a change in *D* provided a larger variation. Figure 3D shows a comparison of all different geometries through the metric $D - d$ (chosen for improved visualization of the results): *D* is proportional to the contact diameter $d_c$ of the membrane with the chamber, and *d* represents the critical value for $d_c$ below which the valve is open. As shown in the figure, there seems to be an optimal value for $D$ - $d$, equal to 8.5 mm with a 500 μm membrane, which minimizes both $\Delta p_{th}$ for each supply pressure level and its variation across supply levels, thereby leading to an overall better performance of the ROM-configured valve.

***Overpressurization protection in a pneumatic soft hand***

The ROM-configured soft valve was embedded in an elastomeric two-finger hand to demonstrate the overpressurization protection capability (Fig. 3E and movie S2). Upon inflation, the fingers bend, making it possible to simulate a handshake for human–robot interaction scenarios. Only one finger had a ROM-configured soft valve at its tip ($D$ = 10 mm, $d$ = 0.8 mm, and membrane thickness $h$ = 500 μm), making it

possible to better highlight the effect of the valve on the behavior of the gripper. The soft valve's control chamber was pressurized first and isolated from the supply. The gripper was then actuated to perform the handshake (Fig. 3F, steps 1 and 2). Once inflated, the soft digits were squeezed powerfully to overpressurize them (step 3). The finger with the soft valve at its tip let air out, deflating further as the grip was tightened. Conversely, the other finger suffered irreversible damage due to plastic deformation of the inflatable membranes at the tip (step 4). Repeating the experiment showed that the behavior of the damaged finger was compromised: the tip of the finger overinflated from the start and the bending angle of the digit was reduced. A second squeeze caused the actuator to burst at the site of the damage (step 5), making it unresponsive, in contrast to the performance of the finger with the soft valve at its tip, which remained unaltered (step 6).

**Two-Stage Soft Valves Achieves Endogenous Control and Fault Isolation**

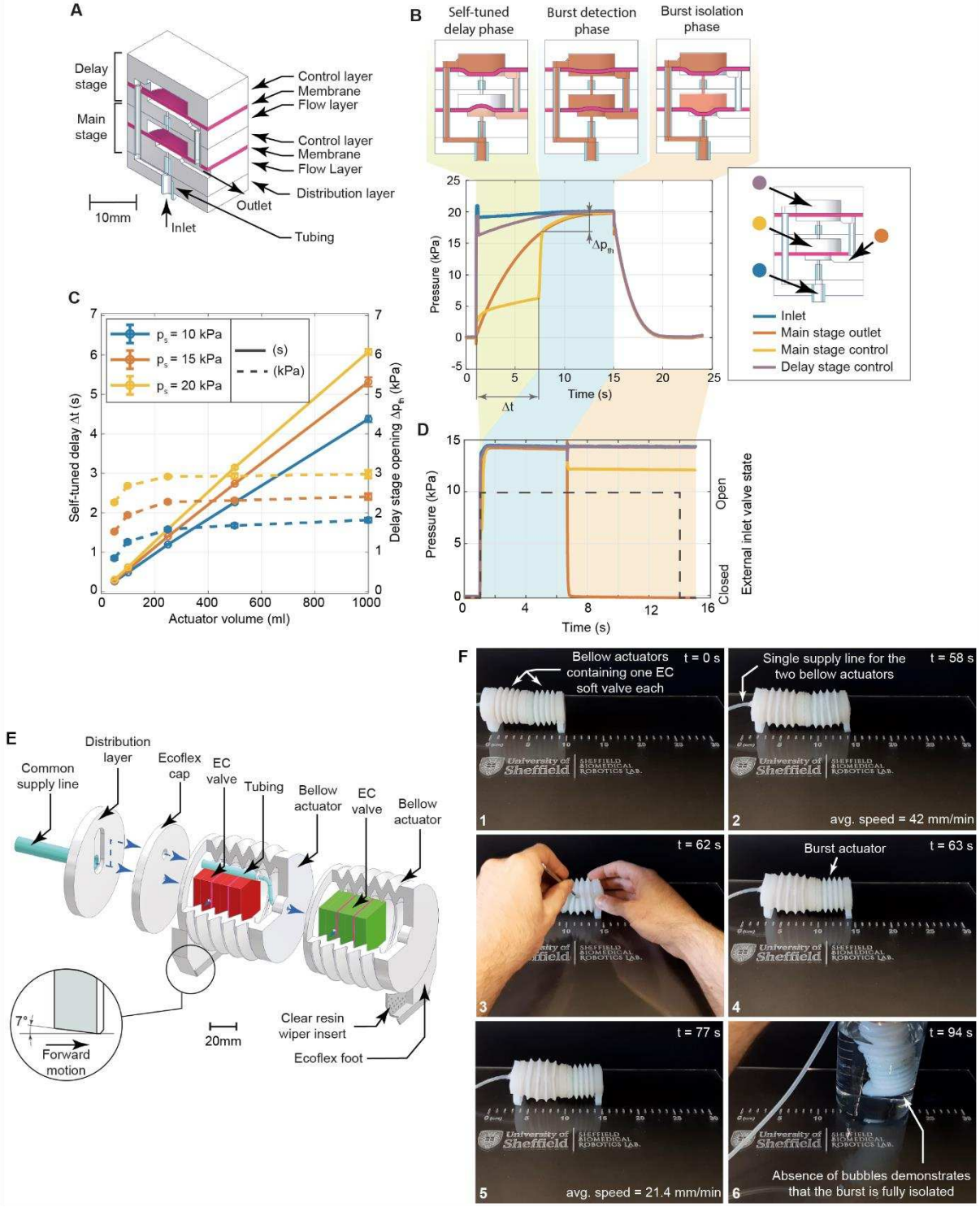


**Fig. 4. EC soft valve characterization and burst isolation demonstration in a soft crawler.** **(A)** Internal structure of the two-stage EC soft valve. The main stage at the bottom ($D$ = 6 mm, $d$ = 0.5 mm, $h$ = 500 μm) is internally connected to the delay stage at the top ($D$ = 10 mm, $d$ = 0.5 mm, $h$ = 500 μm). The EC valve can generate its own control signal thanks to the joint action of the two valves, which enables self-tuning operation. **(B)** Representative experiment used to capture the behavior of the valve in terms of $\Delta p_{th}$ and self-tuned delay time $\Delta t$ with an actuator volume of 1 L. **(C)** $\Delta p_{th}$ and delay $\Delta t$ obtained by varying the supply pressure and the actuator volume between 50 mL and 1.0 L (error bars represent standard deviations). $\Delta t$ increases linearly with the volume from 260 ms to 6.0 s, proving the self-tuning capability of

the soft valve. Following from the ROM characterization, for the same volume, $\Delta p_{th}$ increases with higher supply pressures. When changing the volume at constant $p_s$, $\Delta p_{th}$ remains almost constant, proving that $\Delta t$ is mostly affected by the SIE volume. **(D)** Burst isolation using the two-stage EC valve. A ballooning actuator (see fig. S9 for details) was used for the experiment. The threshold pressure needed to open the delay stage was reached in less than 200 ms, and the valve successfully isolated the burst (t = 8 s). **(E)** Internal structure of the soft crawler integrating two EC soft valves. **(F)** The soft crawler achieves an average moving speed of 42 mm/min with a supply pressure of 12.5 kPa (steps 1 and 2). A sharp blade is used to cut into the side of the front actuator, bursting it (step 3). The burst front actuator is kept isolated by the corresponding EC valve, while the back one operates normally (steps 4 and 5). To prove the successful isolation of the burst, the robot is submerged in water while still being actuated and no air bubbles are observed (step 6).

***Endogenously controlled soft valve characterization***

One challenge that arises at the system level when using soft valves in FOM is knowing when to pressurize the control chamber because its premature actuation can lead to the isolation of the SIE from the supply. The delay required between the pressurization of the two channels depends on multiple factors such as the supply pressure level, overall SIE volume, geometry, and material properties. Extensive system characterization is required, and challenges remain when different SIEs share the same control line. To avoid these problems, two soft valves can be combined into a unit capable of endogenous control signal generation. This behavior is automatic and does not rely on external pressure sensors, valves, or controllers, thereby eliminating the need for an external control channel.

The Endogenously Controlled (EC) soft valve is created by stacking two soft valves in a main stage at the bottom and in a delay stage at the top, operating at a single supply pressure level (Fig. 4A). The principle of operation is illustrated in Fig. 4B with an actuator volume of 1 L. The SIE was deflated, and both membranes started out in their relaxed states (both soft valves were open). Upon activation of the inlet channel (t = 1.0 s), the delay stage control chamber was pressurized immediately. Consequently, the top membrane deformed, closing the valve, and initializing the delay stage in ROM. Meanwhile, the airflow passed through the FOM-configured main stage and reached the SIE, where the pressure started to increase. The increase in the main stage control pressure during this initial phase results from the slowly increasing outlet pressure, which deforms the main stage membrane upward, compressing the air trapped in the control chamber. Once the outlet pressure reached the correct threshold value, the delay stage opened, allowing air to flow through and pressurize the control chamber of the main stage (t $\approx$ 7.5 s). Henceforth, if a burst occurred, the delay stage would autonomously turn to FOM, due to the inversion of the pressure gradient, and the membrane would switch, trapping the air present in the control chamber of the main stage. The main stage would also switch, thus isolating the faulty SIE from the remainder of the system. A main stage with a small chamber diameter ($D$ = 6 mm) and inlet diameter ($d$ = 0.5 mm) was selected to obtain the fastest FOM behavior, whereas a larger chamber diameter ($D$ = 10 mm) was used for the delay stage, to improve the ROM behavior performance.

The delay stage, which starts in ROM, is key to achieving endogenous control, because the control channel of the main stage is pressurized only once the pressure in the SIE reaches a sufficiently high level, independent of the SIE volume, geometry, or material. When voluntarily deflating the SIE, the soft valve would not impede the

deflation as the control channel of the delay stage would depressurize first. To prove that the new EC soft valve can be paired with SIEs of any volume and self-tune its own operation, valves were connected to a wide range of volumes, from 50 mL to 1.0 L (fig. S8). The effect of the SIE volume on $\Delta t$ between the initial pressurization of the inlet channel and the pressurization of the main stage control chamber is shown in Fig. 4C. This effect is evident, with the delay increasing almost linearly from approximately 260 ms to 6.0 s as the volume increased from 50 mL to 1.0 L. Furthermore, the figure shows that an increase in the supply pressure increases the delay $\Delta t$, and the effect becomes more pronounced at larger volumes: a 42 ms difference was observed for a 50 mL volume between 10 kPa and 20 kPa, while at 1.0 L, the difference became 1.7 s. In contrast, the $\Delta p_{th}$ needed for the delay stage to open was almost constant, independent of the volume: the maximum measured difference was less than 1.0 kPa between the smallest and largest volumes, with a supply pressure of 10 kPa. Finally, the opening $\Delta p_{th}$ measured across all volumes and supply pressure levels were consistent with the results obtained previously for the ROM configured simple valve ($D$ = 10 mm, $d$ = 0.5 mm, and $h$ = 500 μm). The automatic burst detection and isolation of the valve was tested by pairing it to ballooning actuators of two different sizes (fig. S9 and movie S3). The results obtained with the smaller of the two (12 mm diameter of a deflated membrane) are shown in Fig. 4D where $\Delta t$ = 0.16 s. The soft valve was able to fully isolate the burst that happened around t = 6.5 s. Following the sudden depressurization of the outlet, the delay stage switched, isolating the main stage control chamber from the outlet (yellow line in Fig. 4D decoupled from the red line after the burst). The main stage also closed, separating the inlet pressure, which remained equal to the supply pressure, from the outlet, which dropped to ambient pressure. As shown in the figure, the main stage control pressure after the burst stabilized at an intermediate pressure value between the supply and ambient pressures. This value depends on the expansion of the control chamber when the main stage switches and the depressurization caused by the air that escapes from the chamber before the delay stage has closed. As the burst can be considered almost instantaneous, the value depends only on the supply pressure and specifics of the valve (internal geometry and material properties) (fig. S9).

***Autonomous burst detection and isolation in a pneumatic soft crawler***

The seamless integration of the EC valve in existing soft robots was demonstrated using a soft crawler manufactured from two bellows-type actuators. The actuators shared the same supply, as shown in Fig. 4E, and were inflated and deflated simultaneously. The crawling motion was enabled by the asymmetric friction provided by the feet, through the combination of its 7° inclination angle and the low-friction wiper insert. The valves were placed inside the empty volume of the actuators to achieve compactness and to simplify the routing of the pneumatic channels.

The crawler was subjected to a pressure of 12.5 kPa for 5.5 s and then partially deflated for 1.2 s, which resulted in an actuation frequency of 0.15 Hz (Fig. 4F and movie S4). The partial deflation of the actuators decreased the crawling speed, but was necessary to keep the internal channels of the EC valves pressurized. Using the aforementioned actuation sequence, the robot achieved an average crawling speed of 42 mm/min (steps 1 and 2). The front bellows actuator was burst suddenly using a sharp blade and the front EC valve switched and isolated it from the supply (step 3). Because of the partial deflation technique, the pressure in the control chamber of the delay stage did not disappear, maintaining the front actuator isolated, while the rear one kept being actuated. Therefore, the robot could continue crawling at a reduced speed of 21.4

mm/min (steps 4 and 5). No changes to the control sequence were required, and no sensors were present onboard, demonstrating the completely passive and autonomous nature of the approach. Finally, the robot was submerged in water (step 6) to demonstrate the absence of air bubbles originating from the burst actuator, further proving its successful isolation.

## DISCUSSION

Soft valves in soft robotic designs have demonstrated the possibility of controlling the behavior of robots without any onboard electronics (*29*, *31*). In addition, they offer the possibility of low-cost manufacturing and tailored performance as well as the potential for monolithic integration, paving the way for fully soft robots. Thus far, very few studies have examined the possibility of using these components for anything besides logic gates in control units. In this study, we presented a multimodal soft valve that endows resilience to soft robots through an embodied, passive, and autonomous approach, without controller interventions. The valve could be easily integrated into existing pneumatic soft robotic designs, with small alterations required during the manufacturing process.

Inspired by the innate mechanisms observed in biological systems, this work explored the possibility of using soft valves to pre-emptively avoid faults, or limit their adverse effects in soft robots, thus providing continuous operation and extended lifespan. In FOM, the soft valve can autonomously detect and isolate bursts in pneumatic SIEs by reacting to the sudden drop in pressure created by the burst itself. The experimental characterization highlighted the effect of critical design parameters, such as the geometry of the inlet channel, on the switching time of the valve, leading to a design that can consistently isolate burst SIEs as fast as 21 ms, which is 12 ms faster than the average duration of a human blink (*47*). This capability makes it possible to fabricate soft robots that can maintain their functionality in case one or more SIEs burst, with only one common inlet channel, drastically reducing the need for external hardware and the complexity of the control logic. In addition, a partial deflation technique similar to that used for the soft crawler can be used to operate the soft robot while maintaining the faulty fingers fully isolated. Swapping the inlet and outlet channels activates the ROM behavior, which can be used to protect against accidental overpressurization. The importance of this capability was demonstrated in a human–robot interaction application. During the experiment, one of the soft actuators plastically deforms prior to bursting, leading to irreparable damage. This type of damage irrecoverably alters the performance of the actuator, with over-inflation of the damaged section; however, it would not be detected by material self-healing approaches because the continuity of the material matrix is not compromised. Therefore, the ROM-configured valve enables a pre-emptive type of resilience, as opposed to the more common ex-post one. The threshold value that toggles the valve can be tuned to specific needs by varying the control pressure and geometrical design parameters.

A common challenge in soft-robot control stems from the hyperelasticity of soft materials, which leads to an accentuated nonlinear behavior upon repeated inflation. Successful control requires prior knowledge of SIEs, achieved either through numerical modeling or extensive experimental training (*48–50*). This limits the usability of the valve in FOM, whereas the ROM behavior is not affected because the control signal is always present. By pairing the FOM and ROM valve configurations, we demonstrated the possibility of creating a soft valve that generates its own control signal, using direct feedback from the SIE it is paired with. Consequently, despite having only one inlet

and one outlet port, the valve can achieve autonomous burst detection and isolation, irrespective of the nonlinear behavior or size of the SIE. For this to occur, the valve's delay stage automatically swaps from ROM to FOM when a burst occurs, which further highlights the importance of the valve's multimodality. The absence of an external control line makes this pneumatic component a truly self-contained solution for soft-robotic resilience, increasing its usability as a drop-in solution in many soft-robotic applications. While only one elastomer was tested in this study, the working principles of the soft valves rely on fluid dynamics rather than material properties. Stiffer materials can therefore be used provided that the supply pressure is increased, which would be justified by the increased stiffness of the soft actuators the valves are paired to.

Although full integration of the soft valves into the body of soft robots was demonstrated in this study, the fabrication currently requires several manual steps which slow down manufacturing and limit accuracy and repeatability. With the increasing availability of soft 3D-printing materials, additive manufacturing techniques can provide solutions, leading to possible monolithic fabrication (*29–31*). The design could be fully replicated with multi-material printers capable of soluble supports. Bridging techniques can also be used, where available, to avoid the use of support material altogether. A second advantage of additive manufacturing techniques entails further miniaturization of the design which might be required to enable the full potential of a distributed fault-resilience approach at larger scales. One drawback of miniaturization may be the reduction in the maximum flow rates through fluidic components, which leads to increased delays and consequent negative effects on system dynamics. However, with thoughtful design, we believe that the local distributed control approach presented in this study may still be beneficial in reducing the reaction times associated with long and narrow supply lines, which are characteristic of complex microfluidic systems. In such systems, minimizing the physical distance between logic and actuation, as demonstrated in this work, is crucial for achieving the fast reaction times required for critical applications such as burst detection and isolation.

The soft valve presented in this study can form a unifying platform for resilient soft robots by integrating passive pre-emptive fault isolation with material healing techniques. Some of the current limitations of approaches based on self-healing materials include time to recovery and inactivity during healing. The FOM-configured soft valve responds to these limitations by providing deflation and isolation of the faulty actuator. Pairing these technologies would result in the creation of soft robots that can operate while their bodies heal from faults. The approach represents an evolution in the fluidic control and resilience of soft robots, a first step toward transforming the common centralized architecture (with one fluidic controller managing the entire robot) into a distributed one (where local control units autonomously manage the resilience of each SIE). The valves provide hard-coded primitive responses to the system, similar to the instinctive reactions humans experience when responding to threats, independent of the higher-level control logic, meant to protect and preserve the welfare of the system as a whole. Building on responsive mechanisms, more complex systems can be developed, in which units can exchange signals and transfer information using fluidics as a medium, expanding on the paradigm presented in (*52*). The inclusion of distributed fault signaling (*21*, *53*) could lead to the possibility of performing system-level behavior changes to compensate for the faulty section of the robot, either temporarily, while the system is healing, or permanently, further improving the overall resilience. In the long term, these approaches, extended by advancements in biodegradable self-healing materials (*19*, *20*, *54*), are expected to enable the creation of robots that can maximize

their life expectancy, recover from multiple faults while carrying out various tasks, and ultimately degrade and provide resources for other organisms or robots. By capitalizing on key intrinsic capabilities of soft robots, such as better adaptation to unstructured environments, and improving on them by adding self-preservation mechanisms, a new generation of life-like machines can be developed, for a more sustainable future.

## MATERIALS AND METHODS

### Objectives and design of the study

The objective of this study is to demonstrate the use of a multimodal soft valve to provide soft robots with resilience against bursts and overpressurization through passive autonomous reactions. The fully soft valve achieves two modes of operation and can be embedded in the body of the soft robots. The combination of the two modes enables the creation of a soft valve which achieves burst detection and isolation without an externally applied control signal. All these modes of the valve are characterized. Two types of grippers and a soft crawling robot were used as practical examples to demonstrate the resilient behaviors enabled by the soft valves. The statistical methods used to consolidate the investigations are stated in the experimental methods described below.

### Fabrication of valves

#### *Single valve fabrication*

The valve consists of three layers molded out of Ecoflex 00-50 (1:1 ratio of parts A and B, mixed for 3 minutes in an ARE-249 Mixer by Thinky). All molds were printed in clear resin using 50 μm resolution on a Form2. The tubing was cut to length and inserted into the inlet channel area, stopping approximately 1 mm before entering the flow layer chamber. Therefore, the membrane interfaces with a smooth continuous surface when deformed, maximizing the sealing potential. The molds were prepared with Ease Release 200 and the silicone was cast and cured at 20°C for 4 h. Once solid, the flow and control layers were unmolded, while the membrane was left untouched to avoid wrinkling. Sil-Poxy glue was uniformly applied to the surface of the flow layer, which was then pressed onto the membrane. Finally, the pair was bonded to the control layer. The glue was applied to the control layer and not the membrane directly, to avoid adhesive on areas that do not require it, with the risk of locally altering the mechanical properties of the membrane.

#### *Two-stage self-tuning valve*

As shown in fig. S10, layers 2 and 3 and layers 4 and 5 were glued together after molding. Once the glue set, a syringe needle (external diameter of 1 mm) was passed through the central holes of components 4 and 5 to ensure that the channel was glue-free. Then, the pairs were joined by gluing layers 3 and 4 together. A wide needle was run through the side channels, cutting the membrane that obstructs them, and the 3D-printed elements 8 and 9 (printed in clear resin on a Form3) were inserted into these. Finally, layers 1 and 7 were added to the stack completing the fabrication process. The main stage had the following geometric parameters: $D$ = 6 mm, $d$ = 0.5 mm, $h$ = 500 μm. For the delay stage, a valve with $D$ = 6 mm, $d$ = 0.5 mm, and $h$ = 500 μm was used.

### Characterization of the valves

An Arduino Nano paired with a custom-designed PCB was used to control the pneumatic hardware during the characterization of the soft valves and for the demo applications. In addition, all sensors were sampled at 10 kHz using a custom-designed data acquisition system capable of simultaneous sampling on eight channels at a 16-bit

resolution. The remaining hardware included five 12 Vdc solenoid valves, five pressure sensors (Honeywell AVX005PGAA5), a volumetric flow sensor (Renesas FS1012-1100-NG), a peristaltic pump, two 5.0 L accumulators, a flow regulator, a 50 mL syringe, tubing (4 mm ID), and Tee tubes. For a detailed description of the hardware required for each experiment, please refer to figs. S11–S14 in the Supplementary Materials. In the figures, V1, V2, V3, V4 and V5 refer to the solenoid valves.

***FOM characterization experiments***

As shown in fig. S11, valve V1 controls the inlet to the flow layer of the soft valve, V2 controls the outlet, and V3 and V4 manage the inlet and outlet of the control channel of the soft valve, respectively. A flow sensor is placed between the soft valve and V2, to record the air flow out of the soft valve. The pressure in the accumulator was stabilized at the target pressure and the pump was switched off, to enable accurate pressure measurements. There were four phases in the experiment: the inlet channel was pressurized first (left flow rate spike in Fig. 2B), followed by the control channel. After 2.0 s, V2 was opened to simulate a burst, connecting the main supply to the atmosphere. After a brief initial air discharge, the membrane inside the soft valve blocked the flow and isolated the main supply. This discharge, which corresponds to the middle spike in the flow sensor signal, was used to evaluate the response time of the valve. The time $\Delta t$ required for the valve to isolate the burst was defined by the intersection between the flow rate (Fig. 2B) and the threshold line. The threshold value was set to 10% higher than the output noise of the flow sensor at rest. The fourth and final step was resetting the pneumatic circuit by depressurizing the channels (right flow rate spike).

Eight designs of the soft valve were manufactured (three samples per design) and tested. Four different membrane thicknesses were produced: 250, 500, 750, and 1000 μm ($d$ = 0.5 mm, $D$ = 10 mm). $d$ was varied from 0.5 to 0.8 to 1.5 mm (constant membrane thickness of 500 μm, $D$ = 10 mm), whereas $D$ was changed from 6 to 8 to 10 mm (constant membrane thickness of 500 μm, $d$ = 0.5 mm). In addition, the supply pressure level $p_s$ was varied from 10 to 30 kPa. The spikes visible in the flow rate data refer to the initial pressurization of the circuit, simulated burst, and reset of the pneumatic circuit before the next experiment. Each data point in the chart represents the average of 15 trials (5 trials for each of the 3 samples per design). The average standard deviations were computed using the formula

$$SD = \sqrt{\frac{1}{3}\left({SD_1}^2 + {SD_2}^2 + {SD_3}^2\right)}.$$

When evaluating whether the membrane thickness had a statistically significant impact on the switching time, separate one-way ANOVA tests were conducted and the five resulting p-values were then averaged to get the final one (table S1). For each supply pressure value, four groups were compared, one for each membrane thickness, and each group contained data from all three samples and all five repetitions (15 data-points in total in each group).

***ROM characterization experiments***

As displayed in fig. S12, valve V1 manages the inlet to the soft valve, V2 manages the outlet, V3 allows the pressurization of the control channel, and V4 allows its deflation. Similar to the FOM experiments, the pressure was stabilized in the tank and the pump was switched off. A 35 mL volume, together with a flow regulator, was used to slow down the pressurization of the inlet channel and allow more precise measurements. These can be considered as the SIE connected to the soft valve. The same membrane thicknesses and internal geometries were used as described previously. Each

experimental trial consists of three phases. Valve V3 was opened to pressurize the control channel. V1 was opened 1.0 s later, allowing air to enter the main channel of the soft valve. The valve opened when the pressure at the inlet of the soft valve reached a threshold value dependent on the control pressure, and the outlet channel was pressurized. At that instant, the difference between the control and inlet pressures determined the opening $\Delta p_{th}$ for the valve in those conditions. The final phase comprised a circuit reset for the next trial. The main inlet valve was closed, the control channel was depressurized, and the outlet valve was opened for 3.0 s. The statistical analysis of the results was conducted as previously described.

***Two-stage valve characterization***

Only two valves were required for characterizing the EC soft valve: V1 controlled the main inlet, while V2 controlled the outlet (fig. S13). A 5.0 L glass container served as the varying SIE volume. Water was used to precisely regulate the air volume within it in the range of 50 mL to 1.0 L. Three soft-valve samples were manufactured and tested at three different supply pressures (10, 15, and 20 kPa). Five trials were performed for each supply pressure level and actuator volume and the results were averaged. The actuator volume was varied from 50 mL to 1.0 L to cover a wide range of soft robotics applications and to better highlight the self-tuning capability of the soft valve. During each experiment, valve V1 was kept open for a sufficiently long time for the actuator volume to reach the supply pressure level. V1 was then closed and V2 was opened to depressurize the actuator and soft valve, resetting the circuit for the next run. For the burst detection and isolation experiments, the outlet reservoir and valve V2 were replaced by the ballooning actuators (fig. S9 and fig. S14).

***Fabrication and control of the soft robots***

The fabrication process for each robot is detailed in the Supplementary Methods section, together with a description of the hardware needed for each demonstration and the corresponding pneumatic circuit.

**Supplementary Materials**

Table S1. Analysis of the p-values obtained by the ANOVA test on $\Delta t$.
Data file S1. CAD models.
Movie S1. Automatic fault detection and isolation in a pneumatic soft gripper.
Movie S2. Passive overpressurization protection in a pneumatic soft gripper.
Movie S3. Endogenously controlled soft valve achieves autonomous burst detection and isolation.
Movie S4. Endogenously controlled soft valve achieves autonomous burst detection and isolation in a pneumatic soft crawler.

**References and Notes**


1. C. S. X. Ng, G. Z. Lum, Untethered Soft Robots for Future Planetary Explorations? *Adv. Intell. Syst.* **5**, 2021–2024 (2023).
2. C. Majidi, Soft-Matter Engineering for Soft Robotics. *Adv. Mater. Technol.* **4**, 1800477 (2019).
3. P. Polygerinos, N. Correll, S. A. Morin, B. Mosadegh, C. D. Onal, K. Petersen, M. Cianchetti, M. T. Tolley, R. F. Shepherd, Soft Robotics: Review of Fluid-Driven Intrinsically Soft Devices; Manufacturing, Sensing, Control, and Applications in Human-Robot Interaction. *Adv. Eng. Mater.* **19**, 1700016 (2017).
4. E. T. Roche, M. A. Horvath, I. Wamala, A. Alazmani, S. E. Song, W. Whyte, Z. Machaidze, C. J. Payne, J. C. Weaver, G. Fishbein, J. Kuebler, N. V. Vasilyev, D. J. Mooney, F. A. Pigula, C. J. Walsh, Soft robotic sleeve supports heart function. *Sci. Transl. Med.* **9**, eaaf3925 (2017).
5. Y. Zhang, P. Li, J. Quan, L. Li, G. Zhang, D. Zhou, Progress, Challenges, and Prospects of Soft Robotics for Space Applications. *Adv. Intell. Syst.* **5**, 2200071 (2023).
6. E. Perez-Guagnelli, J. Jones, A. H. Tokel, N. Herzig, B. Jones, S. Miyashita, D. D. Damian, Characterization, Simulation and Control of a Soft Helical Pneumatic Implantable Robot for Tissue Regeneration. *IEEE Trans. Med. Robot. Bionics*. **2**, 94–103 (2020).
7. D. Rus, M. T. Tolley, Design, fabrication and control of soft robots. *Nature*. **521**, 467–475 (2015).
8. S. Terryn, J. Brancart, D. Lefeber, G. Van Assche, B. Vanderborght, Self-healing soft pneumatic robots. *Sci. Robot.* **2**, eaan4268 (2017).
9. K. Man, A. Damasio, Homeostasis and soft robotics in the design of feeling machines. *Nat. Mach. Intell.* **1**, 446–452 (2019).
10. T. Zhang, W. Zhang, M. M. Gupta, Resilient robots: Concept, review, and future directions. *Robotics*. **6**, 22–36 (2017).
11. J. Bongard, V. Zykov, H. Lipson, Resilient machines through continuous self-modeling. *Science (80-. ).* **314**, 1118–1121 (2006).
12. A. Cully, J. Clune, D. Tarapore, J. B. Mouret, Robots that can adapt like animals. *Nature*. **521**, 503–507 (2015).
13. K. Gilpin, D. Rus, Modular robot systems. *IEEE Robot. Autom. Mag.* **17**, 38–55 (2010).
14. A. Brunete, A. Ranganath, S. Segovia, J. P. de Frutos, M. Hernando, E. Gambao, Current trends in reconfigurable modular robots design. *Int. J. Adv. Robot. Syst.* **14**, 1729881417710457 (2017).
15. S. Li, R. Batra, D. Brown, H. D. Chang, N. Ranganathan, C. Hoberman, D. Rus, H. Lipson, Particle robotics based on statistical mechanics of loosely coupled components. *Nature*. **567**, 361–365 (2019).
16. R. Adam Bilodeau, R. K. Kramer, Self-healing and damage resilience for soft robotics: A review. *Front. Robot. AI*. **4**, 48 (2017).

17. M. J. Ford, C. P. Ambulo, T. A. Kent, E. J. Markvicka, C. Pan, J. Malen, T. H. Ware, C. Majidi, A multifunctional shape-morphing elastomer with liquid metal inclusions. *Proc. Natl. Acad. Sci. U. S. A.* **116**, 21438–21444 (2019).
18. C. E. Diesendruck, N. R. Sottos, J. S. Moore, S. R. White, Biomimetic Self-Healing. *Angew. Chemie - Int. Ed.* **54**, 10428–10447 (2015).
19. M. Baumgartner, F. Hartmann, M. Drack, D. Preninger, D. Wirthl, R. Gerstmayr, L. Lehner, G. Mao, R. Pruckner, S. Demchyshyn, L. Reiter, M. Strobel, T. Stockinger, D. Schiller, S. Kimeswenger, F. Greibich, G. Buchberger, E. Bradt, S. Hild, S. Bauer, M. Kaltenbrunner, Resilient yet entirely degradable gelatin-based biogels for soft robots and electronics. *Nat. Mater.* **19**, 1102–1109 (2020).
20. Z. Wei, J. H. Yang, Z. Q. Liu, F. Xu, J. X. Zhou, M. Zrínyi, Y. Osada, Y. M. Chen, Novel biocompatible polysaccharide-based self-healing hydrogel. *Adv. Funct. Mater.* **25**, 1352–1359 (2015).
21. H. Wang, S. Terryn, Z. Wang, G. Van Assche, F. Iida, B. Vanderborght, Self-Regulated Self-Healing Robotic Gripper for Resilient and Adaptive Grasping. *Adv. Intell. Syst.,* **5***,* 2300223 (2023).
22. T. J. Koh, L. A. DiPietro, Inflammation and wound healing: the role of the macrophage. *Expert Rev. Mol. Med.* **13**, e23 (2011).
23. O. Speck, T. Speck, An Overview of Bioinspired and Biomimetic Self-Repairing Materials. *Biomimetics*. **4**, 26 (2019).
24. S. A. Eming, P. Martin, M. Tomic-Canic, Wound repair and regeneration: Mechanisms, signaling, and translation. *Sci. Transl. Med.* **6** (2014), doi:10.1126/scitranslmed.3009337.
25. E. C. Jensen, W. H. Grover, R. A. Mathies, Micropneumatic digital logic structures for integrated microdevice computation and control. *J. Microelectromechanical Syst.* **16**, 1378–1385 (2007).
26. B. Mosadegh, T. Bersano-Begey, J. Y. Park, M. A. Burns, S. Takayama, Next-generation integrated microfluidic circuits. *Lab Chip*. **11**, 2813–2818 (2011).
27. M. Rhee, M. A. Burns, Microfluidic pneumatic logic circuits and digital pneumatic microprocessors for integrated microfluidic systems. *Lab Chip*. **9**, 3131–3143 (2009).
28. P. N. Duncan, S. Ahrar, E. E. Hui, Scaling of pneumatic digital logic circuits. *Lab Chip*. **15**, 1360–1365 (2015).
29. M. Wehner, R. L. Truby, D. J. Fitzgerald, B. Mosadegh, G. M. Whitesides, J. A. Lewis, R. J. Wood, An integrated design and fabrication strategy for entirely soft, autonomous robots. *Nature*. **536**, 451–455 (2016).
30. S. Wang, L. He, P. Maiolino, A Modular Approach to Design Multi-Channel Bistable Valves for Integrated Pneumatically-Driven Soft Robots via 3D-Printing. *IEEE Robot. Autom. Lett.* **7**, 3412–3418 (2022).
31. Y. Zhai, A. De Boer, J. Yan, B. Shih, M. Faber, J. Speros, R. Gupta, M. T. Tolley, Desktop fabrication of monolithic soft robotic devices with embedded fluidic control circuits. *Sci. Robot.* **8**, eadg3792 (2023).
32. K. L. Dorsey, Electronics-free soft robot has a nice ring to it. *Sci. Robot.* **7**, eabn6551 (2022).
33. V. Cacucciolo, J. Shintake, Y. Kuwajima, S. Maeda, D. Floreano, H. Shea, Stretchable pumps for soft machines. *Nature*. **572**, 516–519 (2019).
34. W. Tang, C. Zhang, Y. Zhong, P. Zhu, Y. Hu, Z. Jiao, X. Wei, G. Lu, J. Wang, Y. Liang, Y. Lin, W. Wang, H. Yang, J. Zou, Customizing a self-healing soft pump for robot. *Nat. Commun.* **12**, 2247 (2021).
35. S. Xu, C. M. Nunez, M. Souri, R. J. Wood, A compact DEA-based soft peristaltic pump for power and control of fluidic robots. *Sci. Robot.* **8**, eadd4649 (2023).

36. F. Perdigones, A. Luque, J. M. Quero, Correspondence between electronics and fluids in MEMS: Designing microfluidic systems using electronics. *IEEE Ind. Electron. Mag.* **8**, 6–17 (2014).
37. S. Song, S. Joshi, J. Paik, CMOS-Inspired Complementary Fluidic Circuits for Soft Robots. *Adv. Sci.* **8**, 2100924 (2021).
38. J. Teichmann, P. Auth, S. Conrad, T. Speck, and F. J. Tauber, An Insect-Inspired Soft Robot Controlled by Soft Valves. *Conference on Biomimetic and Biohybrid Systems*, 428-441 (2023).
39. P. Rothemund, A. Ainla, L. Belding, D. J. Preston, S. Kurihara, Z. Suo, G. M. Whitesides, A soft, bistable valve for autonomous control of soft actuators. *Sci. Robot.* **3**, eaar7986 (2018).
40. D. J. Preston, H. J. Jiang, V. Sanchez, P. Rothemund, J. Rawson, M. P. Nemitz, W. K. Lee, Z. Suo, C. J. Walsh, G. M. Whitesides, A soft ring oscillator. *Sci. Robot.* **4**, eaaw5496 (2019).
41. W. K. Lee, D. J. Preston, M. P. Nemitz, A. Nagarkar, A. K. MacKeith, B. Gorissen, N. Vasios, V. Sanchez, K. Bertoldi, L. Mahadevan, G. M. Whitesides, A buckling-sheet ring oscillator for electronics-free, multimodal locomotion. *Sci. Robot.* **7**, eabg5812 (2022).
42. D. Drotman, S. Jadhav, D. Sharp, C. Chan, M. T. Tolley, Electronics-free pneumatic circuits for controlling soft-legged robots. *Sci. Robot.* **6**, eaay2627 (2021).
43. M. Wehner, M. T. Tolley, Y. Mengüç, Y. L. Park, A. Mozeika, Y. Ding, C. Onal, R. F. Shepherd, G. M. Whitesides, R. J. Wood, Pneumatic Energy Sources for Autonomous and Wearable Soft Robotics. *Soft Robot.* **1**, 263–274 (2014).
44. M. Pontin, S. Miyashita, D. D. Damian, Development and Characterization of a Soft Valve for Automatic Fault Isolation in Inflatable Soft Robots. *2022 IEEE 5th Int. Conf. Soft Robot. RoboSoft 2022*, 62–67 (2022).
45. C. Bosio, D. Zrinscak, C. Laschi, M. Cianchetti, Soft Mini Fuse Valve for Resilient Fluidically-Actuated Robots. *IEEE Robot. Autom. Lett.* **8**, 2716–2723 (2023).
46. R. F. Shepherd, F. Ilievski, W. Choi, S. A. Morin, A. A. Stokes, A. D. Mazzeo, X. Chen, M. Wang, G. M. Whitesides, Multigait soft robot. *Proc. Natl. Acad. Sci. U. S. A.* **108**, 20400–20403 (2011).
47. K. A. Kwon, R. J. Shipley, M. Edirisinghe, D. G. Ezra, G. Rose, S. M. Best, R. E. Cameron, High-speed camera characterization of voluntary eye blinking kinematics. *J. R. Soc. Interface*. **10**, 20130227 (2013).
48. P. Schegg, C. Duriez, Review on generic methods for mechanical modeling, simulation and control of soft robots. *PLoS One*. **17**, e0251059 (2022).
49. G. Mengaldo, F. Renda, S. L. Brunton, M. Bächer, M. Calisti, C. Duriez, G. S. Chirikjian, C. Laschi, A concise guide to modelling the physics of embodied intelligence in soft robotics. *Nat. Rev. Phys.* **4**, 595–610 (2022).
50. M. Grube, J. C. Wieck, R. Seifried, Comparison of Modern Control Methods for Soft Robots. *Sensors*. **22**, 9464 (2022).
51. Y. S. Lee, N. Bhattacharjee, A. Folch, 3D-printed Quake-style microvalves and micropumps. *Lab Chip*. **18**, 1207–1214 (2018).
52. C. A. Aubin, S. Choudhury, R. Jerch, L. A. Archer, J. H. Pikul, R. F. Shepherd, Electrolytic vascular systems for energy-dense robots. *Nature*. **571**, 51–57 (2019).
53. S. K. Tabrizian, F. Sahraeeazartamar, J. Brancart, E. Roels, P. Ferrentino, J. Legrand, G. Van Assche, B. Vanderborght, S. Terryn, A Healable Resistive Heater as a Stimuli-Providing System in Self-Healing Soft Robots. *IEEE Robot. Autom. Lett.* **7**, 4574–4581 (2022).
54. A. Costa Cornellà, S. K. Tabrizian, P. Ferrentino, E. Roels, S. Terryn, B. Vanderborght, G. Van Assche, J. Brancart, Self-Healing, Recyclable, and Degradable Castor Oil-Based Elastomers for Sustainable Soft Robotics. *ACS Sustain. Chem. Eng.* **11**, 3437–3450 (2023).

**Acknowledgments:** We thank Shuhei Miyashita for valuable discussions and Roderich Gross, Sanja Dogramadzi for reviewing our manuscript. We thank Joanna Jones, Freddy Forbes , Kaan Esendag, MennaHalla HA Mahmoud and Jialun Liu for their input to the manuscript. For the purpose of open access, the authors have applied a Creative Commons Attribution (CC BY) licence to any Author Accepted Manuscript version arising.

**Funding:**

Engineering and Physical Science Research Council DTP PhD Scholarship (MP)
Engineering and Physical Science Research Council EP/X017486/1 (DD)

**Author contributions:**

Conceptualization: MP, DD
Methodology: MP, DD
Investigation: MP
Visualization: MP, DD
Funding acquisition: MP, DD
Project administration: MP, DD
Supervision: DD
Writing – original draft: MP, DD
Writing – review & editing: MP, DD

**Competing interests:** Authors declare that they have no competing interests.

**Data and materials availability:** All (other) data needed to evaluate the conclusions in the paper are present in the paper or the Supplementary Materials. The data for this study have been deposited in the database at https://doi.org/10.15131/shef.data.25136975.v1.

# SUPPLEMENTARY METHODS

## Additional FOM characterization experiments

### *FOM operation under valve deformation*

In order to characterize the behavior of the FOM-configured soft valve when deformed, experiments were conducted by progressively loading the valve (in 50 g increments) orthogonally to the inlet channel, so as to cause the membrane to buckle (fig. S4A). With the valve loaded this way, FOM experiments were run (refer to Materials and Methods section and fig. S11 for details) to measure the switching time of the valve, either until it failed the burst isolation experiment (fig. S4C) or a maximum of 1.2 kg was applied. Two membrane thicknesses were used, 250 μm and 1000 μm ($D$ = 10 mm, $d$ = 0.5 mm in both cases), and two valves for each thickness were tested. Each valve was subjected to progressive loading 5 times and the loads were completely removed between each trial. A low $p_s$ =10 kPa was used during the trials, to create the most difficult switching conditions for the valves. The thinnest membrane (250 μm) was tested as it buckles more easily, while the 1000 μm membrane variant was selected as it is the most difficult valve to switch at low supply pressure.

Six additional experiments were conducted to evaluate the behavior of the valve once the external load is removed. Three experiments were conducted with a 1 kg load present from the start and then removed after the simulated burst, while another three were run with the load placed on the valve after the simulated burst and removed shortly thereafter.

### *Valve's FOM lifetime*

The lifetime of the soft valve was characterized by repeatedly performing FOM experiments (using the circuit in fig. S11) and measuring the valve's switching time as described in the Materials and Methods section. Valves with 250 μm membranes were utilized and supplied with $p_s$ =30 kPa to maximize strains and stresses within the membranes (shortest lifespan). The results are shown in fig, S5 for 3 valves where experiments were stopped when valves failed or after 5000 switching cycles were completed.

## Fabrication of the robots

### *Fabrication of the 5-finger gripper*

All elements were cast from Ecoflex 00-50 (for preparation, refer to the valve manufacturing process) and bonded using Sil-Poxy glue. Each finger is a Pneu-Net-type actuator composed of two layers, whereas the palm of the gripper, which contains five soft valves, is composed of four layers (Fig. 2G). Tubing was placed in the relevant areas of the molds before casting the silicone, and the layers were then glued together individually. The palm was tested to ensure that all channels were unobstructed, before gluing the pre-assembled soft fingers in place, one at a time.

### *Fabrication of the 2-finger hand*

This procedure is similar to that followed for the 5-finger gripper. The molds were prepared by placing tubing to create the internal channels, followed by spraying with a releasing agent. There are four main elements in the design: the palm, the two fingers, and the ROM-configured valve (Fig. 3E). The fingers and the valve were assembled first and then the fingers were bonded to the palm. The gripper and valve

were tested to ensure that all channels worked correctly, and the valve was glued at the tip of the soft finger that had the control channel.

### *Fabrication of the soft crawler*

To create the soft crawler, two EC soft valves were manufactured following the technique previously described. The molds for the bellows actuators, the feet, the distribution layer and the cap were 3D-printed out of PLA on a Prusa Mk3S. All molds were sprayed with Ease Release before casting the Ecoflex 00-50 silicone; the wiper inserts, printed in clear resin on a Form2 printer, were laid in place in the foot molds mid-casting. Once cured, the front EC valve was bonded to the rear bellows actuator using Sil-Poxy glue. The front bellows actuator was then glued to the rear one, and the rear EC valve was bonded to the cap. The tubing connecting the front EC valve and the distribution layer was then routed inside the rear bellows, before the cap, bearing the rear EC valve, was connected using Sil-Poxy. Finally, the distribution layer was glued in place, followed by the feet.

## Control and characterization of robots

### *Burst isolation in a five-finger soft-gripper*

The circuit shown in fig. S15 was used for the fault isolation experiment in the five-finger soft gripper. Four solenoid valves are required to control the pressurization and depressurization of the fingers and the control channel, respectively. The inlet valve V1 was opened for 10.0 s to inflate the gripper. Valve V3 was then activated to pressurize the control channel. This staggered actuation of the channels is required as single stage soft valves were used for this experiment. After 2.0 s, both V1 and V3 were closed, fully isolating the gripper from the supply. One or more fingers were then repeatedly burst using a knife to showcase the burst detection and isolation capability.

### *Overpressurization protection in a soft hand*

The circuit shown in fig. S16 is required for the over-pressurization protection experiment. Valves V2 and V3 control the inflation of the two soft fingers. Valve V1 manages the control channel of the soft valve connected to one of the soft fingers, whereas V4 acts as the common deflation channel. The two soft fingers were managed independently for demonstration purposes. In real world applications, both fingers would have a soft valve at the tip and only one supply line and one control line would be required. During the experiment, V1 was opened and closed after 2.0 s. The fingers were then inflated. Pressure sensor P1 was used to isolate the gripper from the supply when the pressure in the fingers reached a value which, according to the ROM characterization experiments, was not sufficient to trigger the opening of the soft valve for the control pressure used. This setup made it possible to only use one supply pressure level, instead of separate ones for control and inflation pressures. When the pressure in the fingers dropped below the threshold pressure, valves V2 and V3 were opened again, triggering the reinflation of the gripper.

### *Burst isolation in soft crawler*

The inflation and deflation of the robot were managed through valves V1 and V2 (fig. S17). The repeating actuation sequence has a period of 6.7 s. The robot was connected to a supply pressure of 12.5 kPa for 5.5 s and then deflated for 1.2 s. The partial deflation kept the delay stage control chambers of the EC soft valves pressurized, making it possible to maintain the burst actuator isolated, while still controlling the other one

## SUPPLEMENTARY MATERIALS

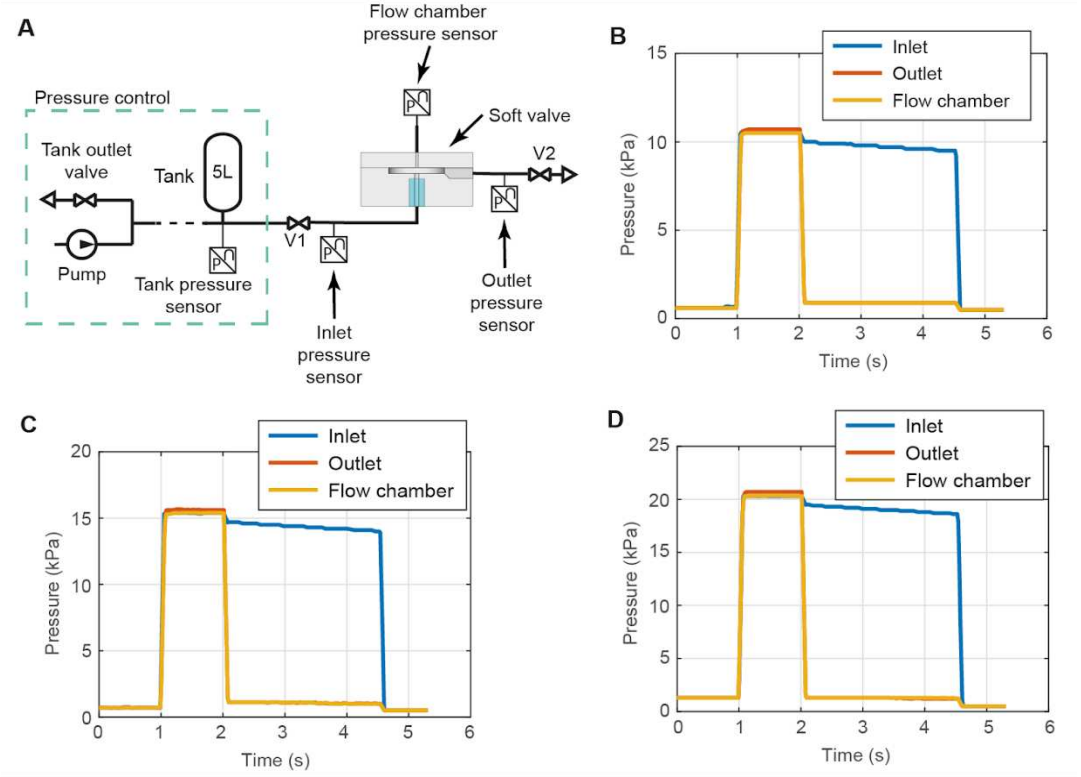


**Fig. S1. Decoupling action of the soft valve. (A)** Pneumatic circuit used for the experiment. The test sample is a version of the soft valve with an inlet channel diameter of 0.5 mm and a chamber diameter of 10 mm, without the membrane and the control layer. A pressure measurement port is used to measure the pressure in the flow chamber, at the exit of the inlet channel. **(B-D)** Experiments that show, for various supply pressure levels, the decoupling effect that, upon a burst, the inlet channel resistance has. The inlet valve V1 is opened at t = 1.0 s. The outlet valve V2 is opened at t = 2.0 s to simulate a sudden burst; the outlet pressure immediately drops to almost ambient pressure levels, whereas the inlet pressure remains close to the supply pressure value. The slight decrease in inlet pressure from 2.0 s onwards is due to the 5.0 L tank discharging through the soft valve and V2.

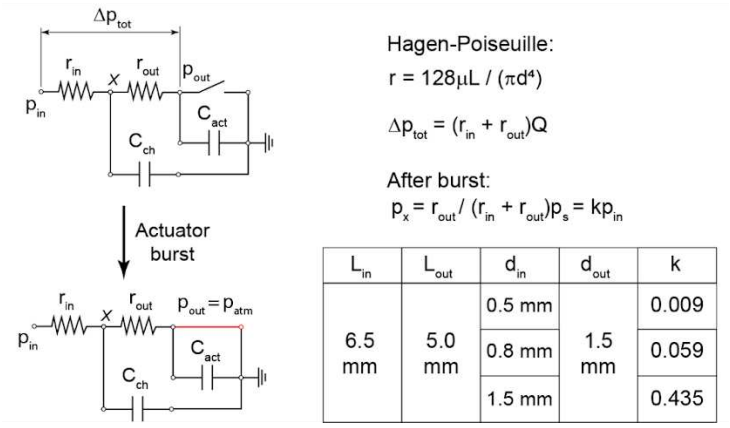


| $L_{in}$ | $L_{out}$ | $d_{in}$ | $d_{out}$ | k |
|---|---|---|---|---|
| 6.5 mm | 5.0 mm | 0.5 mm | 1.5 mm | 0.009 |
| | | 0.8 mm | | 0.059 |
| | | 1.5 mm | | 0.435 |

**Fig. S2. Zero-order model of the FOM valve connected to a soft actuator.** The simplified model neglects the effect of the supply line. A burst in the actuator can be assimilated to a sudden short circuit that forces the outlet pressure $p_{out}$ to ambient pressure level. Point X in the circuit represents the inside of the flow layer chamber, while $r_{in}$ and $r_{out}$ are respectively the inlet and outlet resistances of the soft valve. $C_{act}$ is the capacitive effect associated with the soft actuator, and $C_{ch}$ is that of the flow layer chamber, negligible compared to $C_{act}$. The Hagen-Poiseuille law can be applied in the assumption of laminar air-flow (maximum Reynolds number Re < 2000). As a result, assuming a constant chamber diameter $D$ = 10 mm, it is possible to estimate the pressure underneath the membrane for the various designs that were tested in the study. After a burst, the pressure $p_X$ varies from 43.5% of the inlet pressure, with the widest inlet channel, to just 0.9% of the inlet pressure, when $d$ is equal to 0.5 mm.

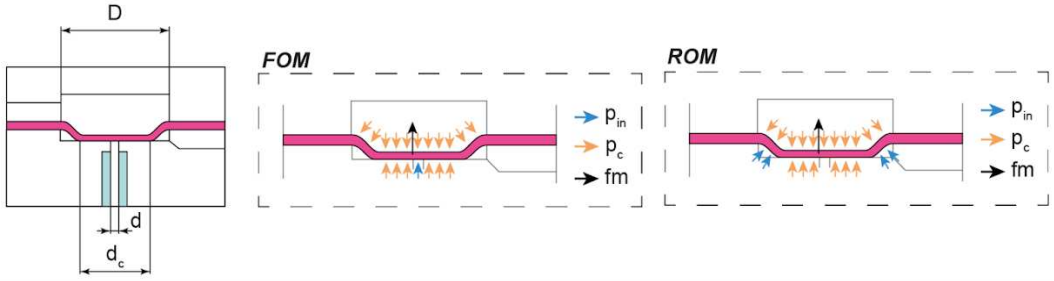


**Fig. S3. Simplified free body diagram of the membrane in FOM and ROM.** The simplified representation neglects the effect of the weight of the membrane itself and lumps the distributed effects of internal stresses within the membrane in the elastic reaction term *fm*.

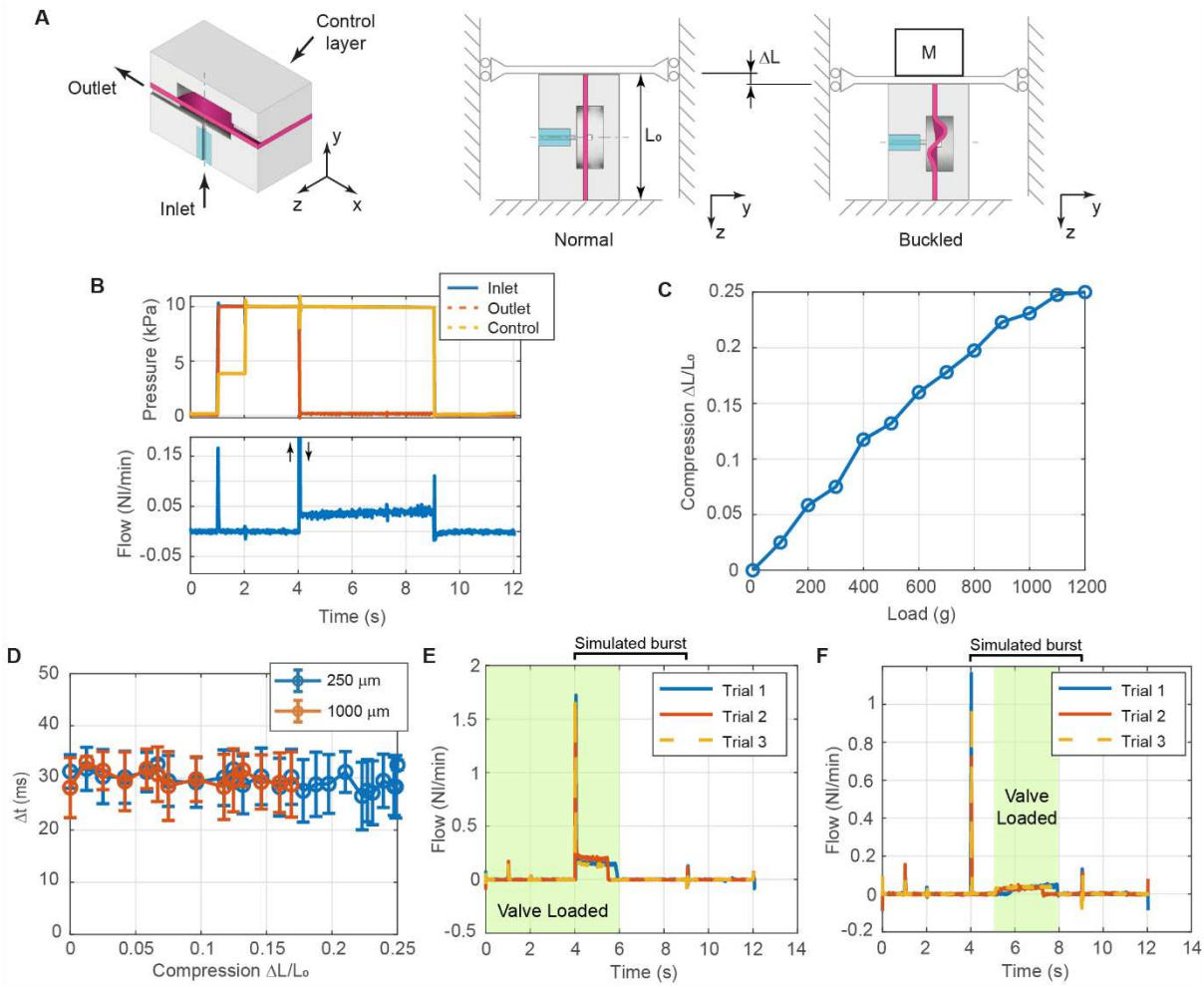


**Fig. S4. FOM operation under deformation. (A)** Valves loaded orthogonally, to induce membrane buckling. **(B)** Example of a failed FOM experiment with a 1000 μm valve loaded with 900 g. After the outlet valve is opened, t = 4 s, some residual outflow is observed. **(C)** Deformation of the valve at increasing loading conditions, expressed as a function of $\Delta L/L_0$. **(D)** Switching time of the deformed valves. The 250 μm variant successfully switched up to the maximum tested loading condition of 1.2 kg. With a 1000 μm membrane, the behavior became unpredictable past 650 g, with some experiments failing at 700 g and some others reaching 850 g before failure. Each error bar represents the standard deviation of a total of 10 trials, averaged as described in the Materials and Methods section. The level of deformation does not seem to affect the switching time, until the valves fail to switch altogether. **(E)** Three FOM experiments showing a 1000 μm membrane valve, initially deformed (1 kg load), successfully isolating bursts once the external load is suddenly removed. **(F)** Three FOM experiments where a 1 kg load is applied to a soft valve (1000 μm membrane) after the initial successful switching. When the valve is deformed, it partially opens, leading to some outflow. The valve successfully closes back up once the load is removed.

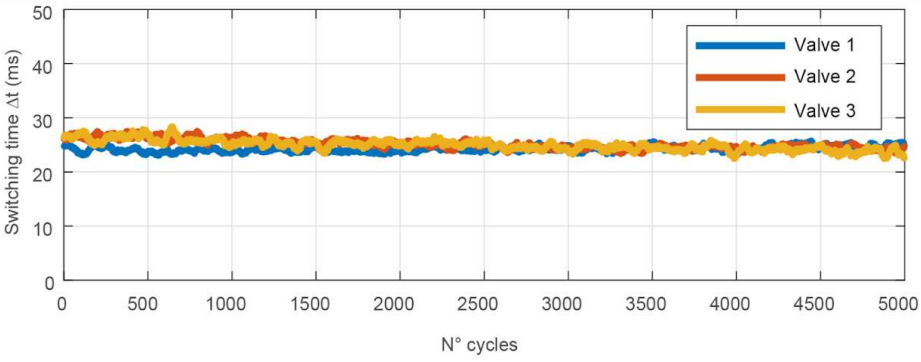


**Fig. S5. Lifetime characterization results.** The results show the FOM switching times of three soft valves equipped with 250 µm membranes and supplied at 30 kPa (thinnest membrane, subject to highest strains). All valves survived the 5000 switching cycles without any noticeable change in performance. The results are plotted using a moving average filter with a window size of 50 samples.

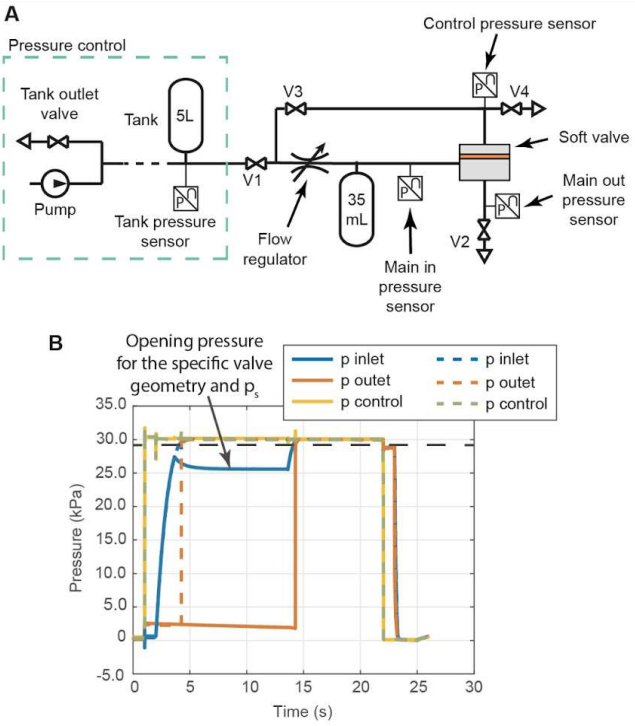


**Fig. S6. Stability of the ROM behavior. (A)** Pneumatic test circuit used for the experiment. **(B)** Experimental results. The dashed lines refer to an experiment where a soft valve ($D$ = 10 mm, $d$ = 1.5 mm, $h$ = 500 µm) is tested using the ROM procedure as detailed in the Materials and methods section and $p_s$ = 30 kPa. As visible, when the inlet pressure reaches the threshold pressure for the valve to open (black dashed line), the outlet pressure instantly jumps to the inlet pressure value (valve open). The solid lines refer to an experiment where the external inlet valve is closed before the soft valve inlet pressure reaches the ROM switching threshold for the valve. The external valve is then kept closed for 10.0 s during which the soft valve remains closed (no relevant changes were observed in the outlet pressure). The external inlet valve is then reopened and, once the soft valve inlet pressure reaches the threshold value, the outlet pressure jumps to the inlet pressure value (soft valve open).

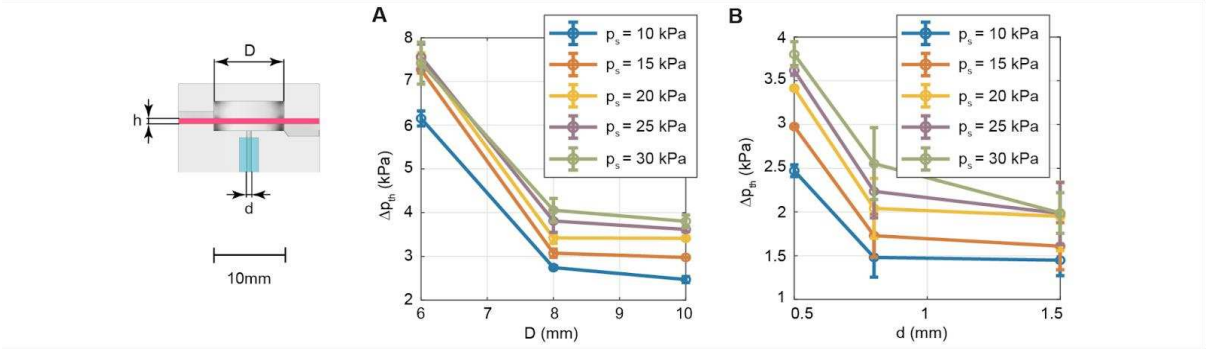


**Fig. S7. Effect of channel geometry on the ROM. (A)** Changing the chamber diameter $D$ from 6mm to 10mm ($d$ = 0.5 mm, $h$ = 500 µm) impacts the behavior of the valve: larger chambers provide more uniform behavior across the range of supply pressures tested, making for a better performing valve overall. Error bars in plots indicate the average standard deviation obtained in the trials (refer to the Materials and Methods section for details). **(B)** Effect of the outlet diameter $d$ on $\Delta p_{th}$ ($D$ = 10 mm, $h$ = 500 µm).

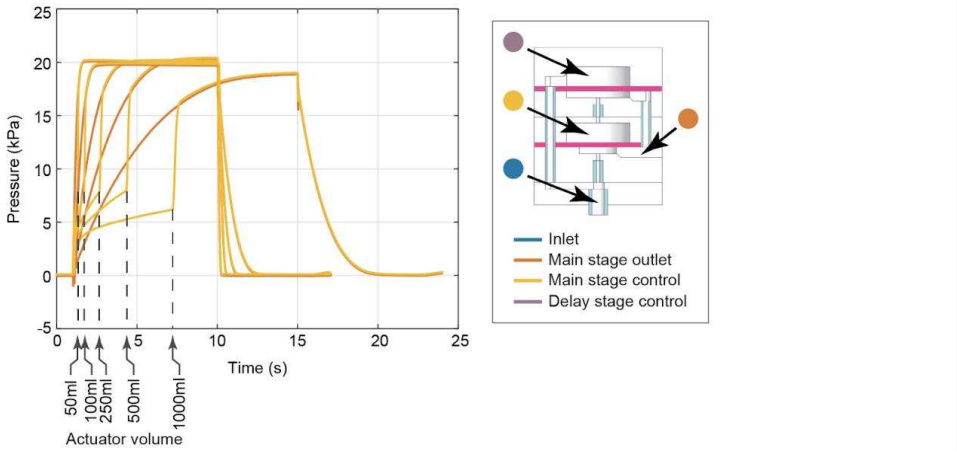


**Fig. S8. EC valve behavior with different actuator volumes.** Pressure profiles highlighting the change in behavior of the EC valve with increasing SIE volumes, with a constant supply pressure of 20 kPa. Only the main stage outlet and control pressures are shown for clarity. The delay time $\Delta t$ increases with actuator volume whereas $\Delta p_{th}$ remains almost constant.

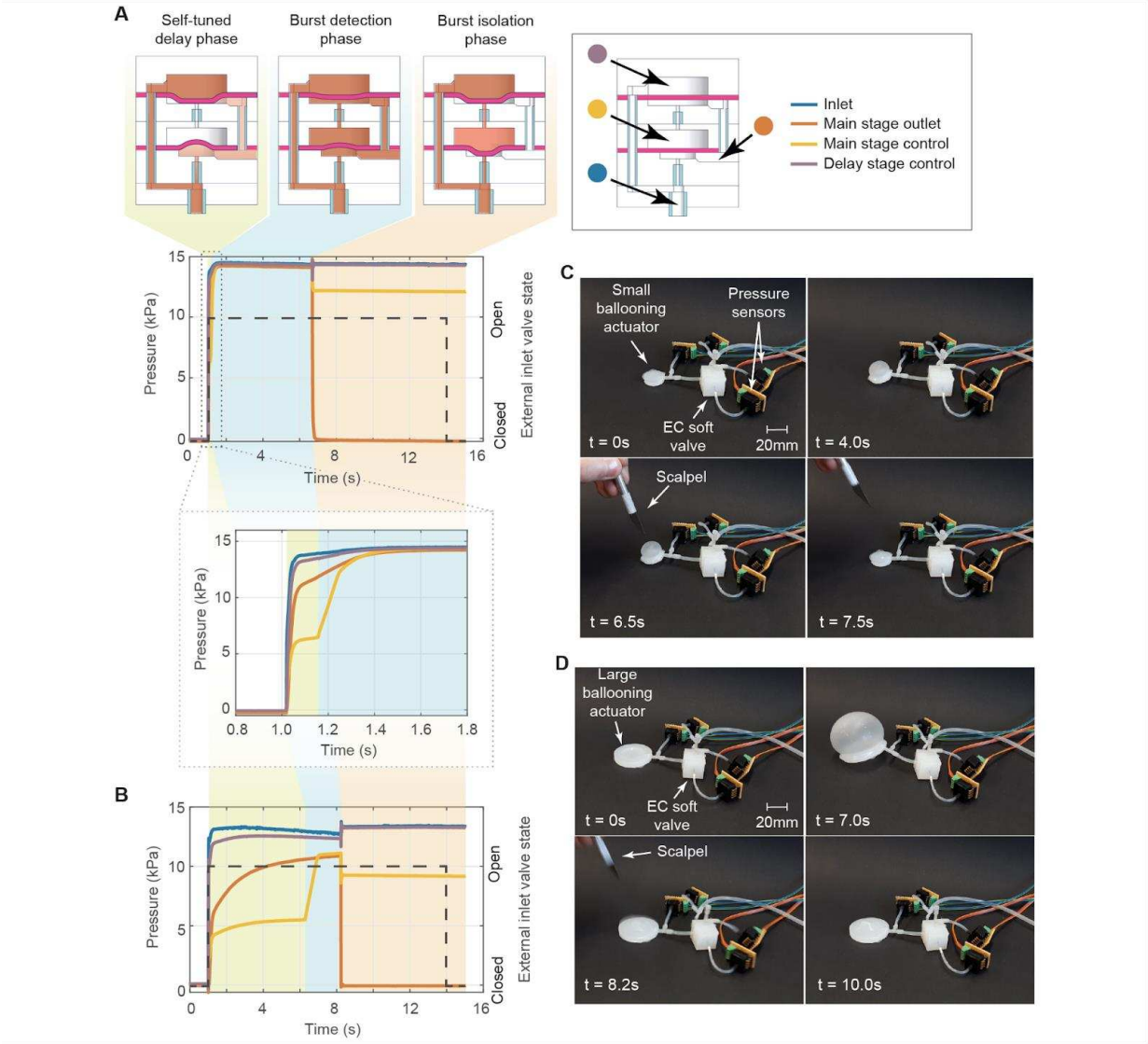


**Fig. S9. Automatic burst detection and isolation with the EC soft valve. (A-B)** Behavior of the two-stage EC valve with burst isolation demonstration. Two ballooning actuators of different sizes are used to compare the behaviors. With the small actuator (deflated membrane measuring 12 mm in diameter) (A), $\Delta p_{th}$ was reached in 160 ms, while it took around 5.0 s with the larger one (24 mm membrane diameter) (B), due to the different pressurization transient of the actuator. The soft valve was capable of automatically detecting and isolating both bursts instantaneously. Immediately after the bursts, the drops in pressure observed in the main stage control chamber between the two experiments were similar. As the burst can be considered almost instantaneous, these depend only on the supply pressure and specifics of the valve (internal geometry and material properties). **(C)** Experiment with the small ballooning actuator corresponding to (A). **(D)** Experiment with the large ballooning actuator corresponding to (B).

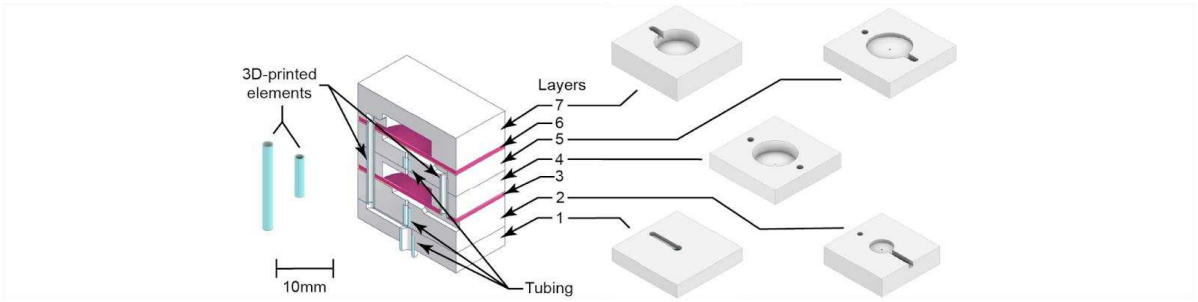


**Fig. S10. Manufacturing of the EC soft valve.**

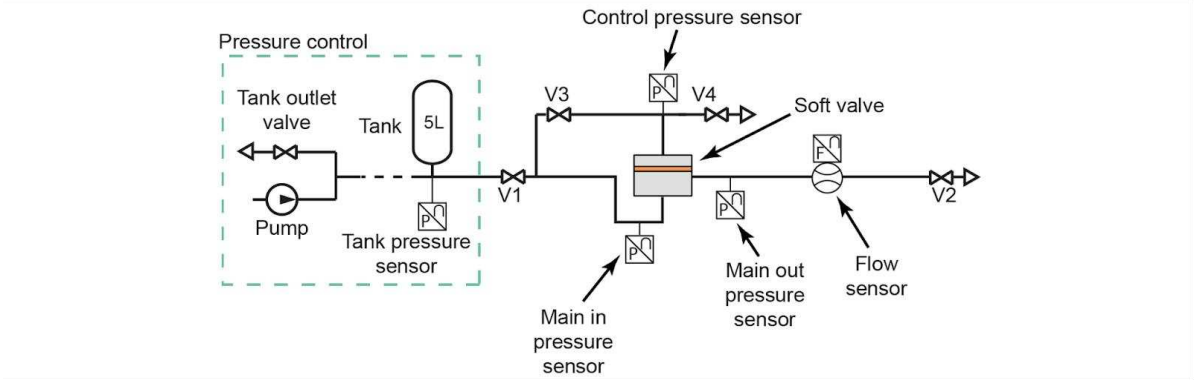


**Fig. S11. Test circuit needed for the FOM characterization.**

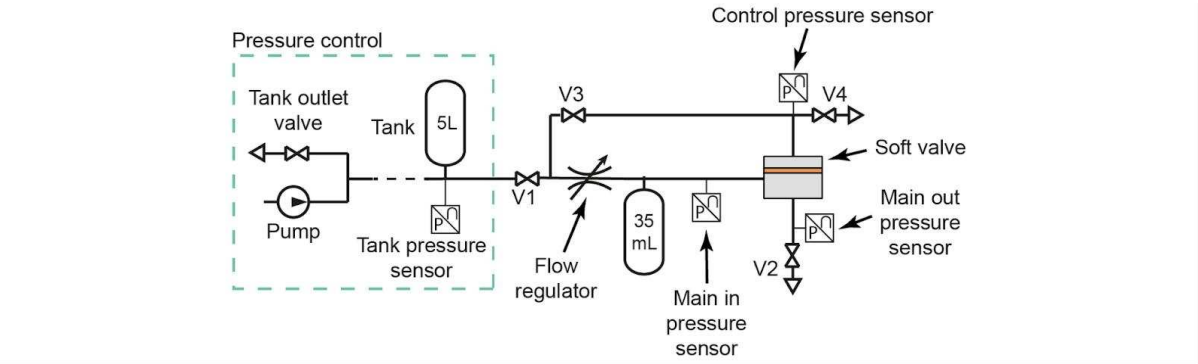


**Fig. S12. Test circuit needed for the ROM characterization.**

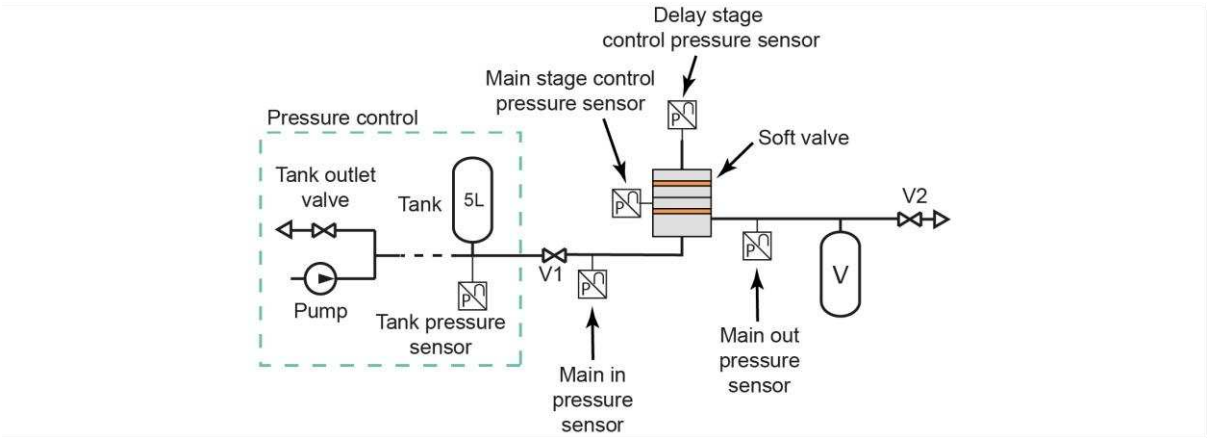


**Fig. S13. Test circuit needed for the EC valve characterization.**

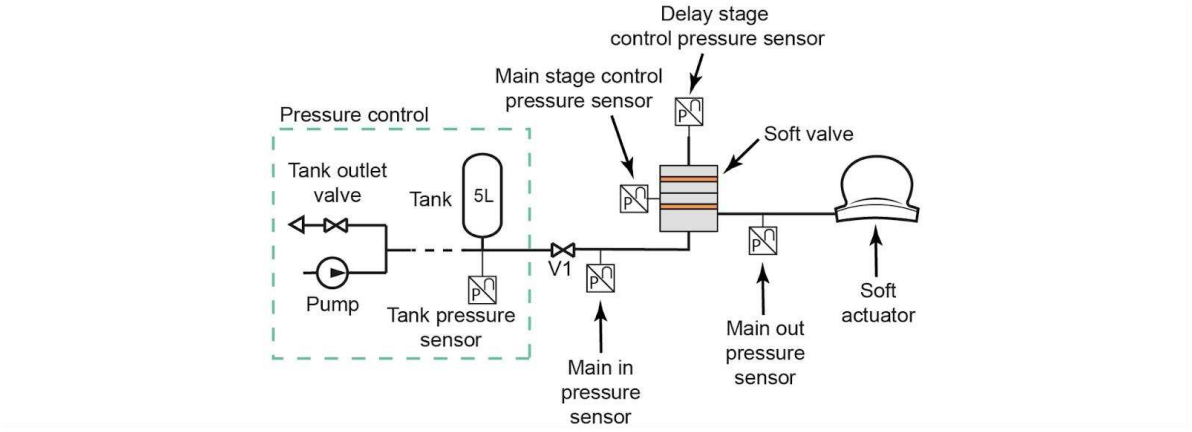


**Fig. S14. Test circuit needed for the EC valve burst isolation experiments.**

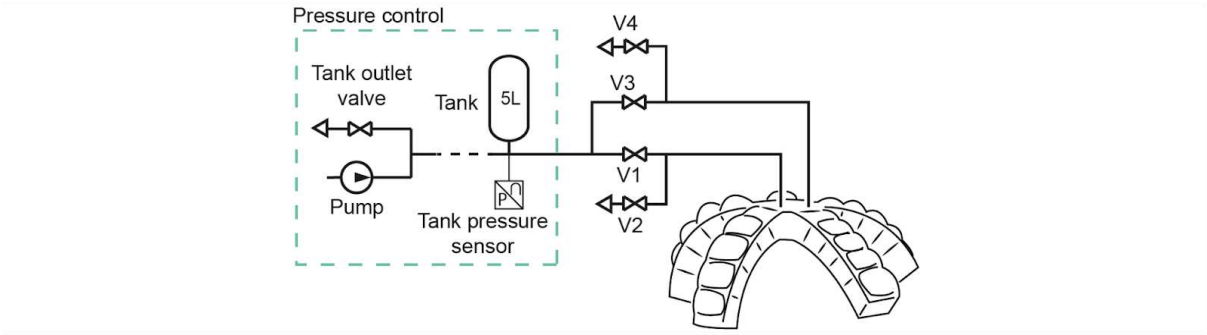


**Fig. S15. Pneumatic circuit for controlling the 5-finger gripper.**

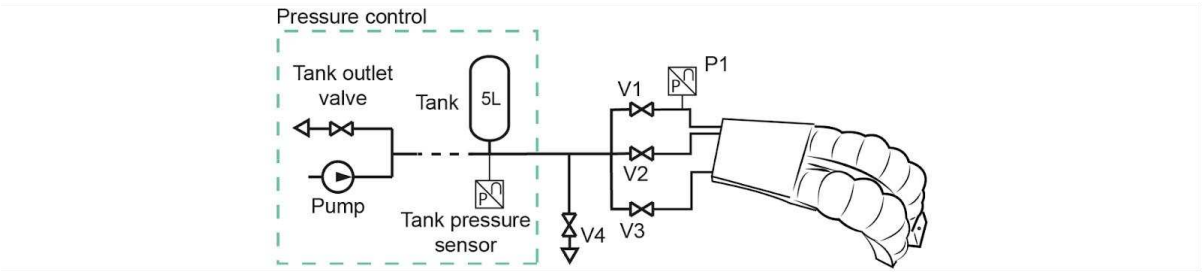


**Fig. S16. Pneumatic circuit for controlling the 2-finger soft hand.**

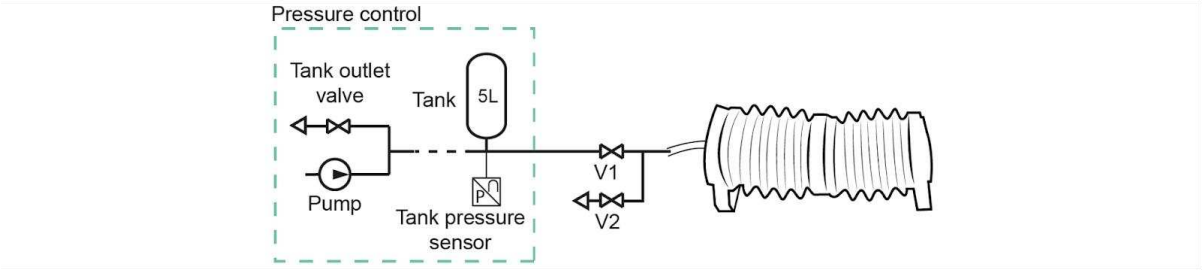


**Fig. S17. Pneumatic circuit for controlling the resilient soft crawler**

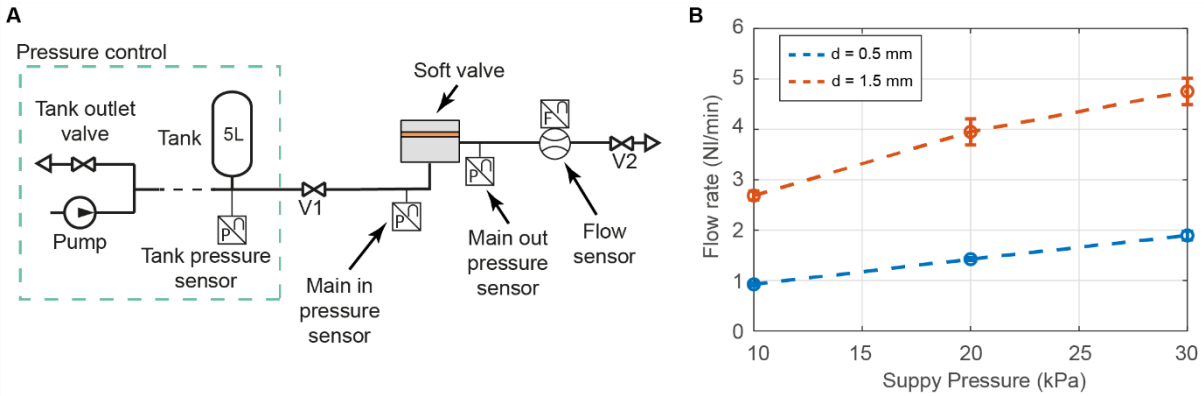


**Fig. S18. Flow rate characterization experiment. (A)** Pneumatic circuit used for the test. **(B)** The two versions of the valve with extremes inlet diameter values, $d$ = 0.5 mm and $d$ = 1.5 mm, were tested to evaluate their flow rates. For each supply pressure value (three in total) three repetitions were conducted. Error bars in the figure represent standard deviations.

| | | ANOVA P-values | |
|---|---|---|---|
| | | **All membranes** | **W/o 250 μm membrane** |
| **Supply pressure $p_s$ (kPa)** | 10 | 0.001 | 0.10 |
| | 15 | 0.02 | 0.82 |
| | 20 | 0.001 | 0.43 |
| | 25 | 0.70 | 0.85 |
| | 30 | 0.40 | 0.29 |
| | **Average** | **0.22** | **0.50** |

**Table S1. Analysis of the p-values obtained by the ANOVA test on $\Delta t$.** The 250 μm membrane shows a statistically significant effect on $\Delta t$ for supply pressures of 10 kPa and 20 kPa. Overall though, the average p-value is 0.22. Excluding the 250 μm membrane, the other membranes do not show significantly different behaviors between one another, for any supply pressure level.

**Movie Legends:**

**Movie S1:** Application experiment showcasing the burst detection and isolation capability of the FOM configured soft valve in a 5-finger soft gripper. The resilient gripper, embedding five soft valves in its palm, has a single supply line and can maintain its grasp on various objects even after multiple fingers are burst.

**Movie S2:** Application experiment showcasing the overpressurization protection capability of the ROM configured soft valve. A 2-finger soft hand is used to simulate a handshake in a human-robot interaction task. One of the fingers is protected by a ROM soft valve, while the other is not. During the experiment, the unprotected finger plastically deforms, suffering irreversible damage, and subsequently bursts, becoming irresponsive. The protected finger does not suffer any damage as the soft valve autonomously releases the excess pressure.

**Movie S3:** Experiment demonstrating the burst detection and isolation capability of the endogenously controlled (EC) soft valve paired with ballooning actuators of different sizes. No external control line is present and only one input, the supply pressure, is provided to the system. The EC valve generates its own control signal, adapting to the inflation transient of the actuators, and achieves autonomous fault detection and isolation when the actuators are burst using a sharp knife.

**Movie S4:** Application experiment showcasing the burst detection and isolation capability of the EC soft valve with a resilient soft crawler. The soft robot, consisting of two bellows-type actuators, embeds two EC soft valves and receives a shared supply pressure signal as its only external input. After an initial crawling sequence, one of the bellows is burst, but the robot keeps advancing using its remaining actuator. The fault is autonomously and fully isolated by the EC valve, as demonstrated by the absence of air bubbles originating from the cut in the bellows when the robot is submerged in water.